



# OCT angiography and its retinal biomarkers [Invited]

TRISTAN T. HORMEL<sup>1</sup> AND YALI JIA<sup>1,2,\*</sup>

<sup>1</sup>Casey Eye Institute, Oregon Health & Science University, Portland, Oregon, USA

<sup>2</sup>Department of Biomedical Engineering, Oregon Health & Science University, Portland, Oregon, USA

\*jiaya@ohsu.edu

**Abstract:** Optical coherence tomography angiography (OCTA) is a high-resolution, depth-resolved imaging modality with important applications in ophthalmic practice. An extension of structural OCT, OCTA enables non-invasive, high-contrast imaging of retinal and choroidal vasculature that are amenable to quantification. As such, OCTA offers the capability to identify and characterize biomarkers important for clinical practice and therapeutic research. Here, we review new methods for analyzing biomarkers and discuss new insights provided by OCTA.

© 2023 Optica Publishing Group under the terms of the [Optica Open Access Publishing Agreement](#)

## 1. Introduction

Many ocular retinal diseases are either vascular in origin or include a vascular component. In such diseases, detecting vascular biomarkers is key to therapeutic research, understanding disease etiology and pathophysiology, and clinical practice. The most common imaging modalities employed to detect vascular biomarkers are fundus photography, dye-based angiography, and OCT angiography (OCTA). Of these, OCTA has several relative advantages. Only OCTA achieves capillary scale resolution. This means that pathology that afflicts capillaries, such as capillary dropout, is best imaged with OCTA. OCTA also obtains higher vascular contrast than fundus photography and is not disrupted by the dye leakage that can obscure vessels in dye-based angiography. All of these aspects are advantageous not only for detecting but also for quantifying vascular pathologies using OCTA. Furthermore, OCTA is uniquely capable of providing depth-resolved biomarkers. Combining these relatively powerful biomarker detection capabilities with non-invasive procedures makes OCTA an extremely promising screening technology for clinical practice.

OCTA is a rapidly developing imaging modality, and OCTA is currently providing new insights into retinal function all the time. This review aims to cover state-of-the-art OCTA-based vascular biomarker detection and quantification. To this end, we begin with a brief review of OCTA signal and image generation so that the advantages and limitations of OCTA-based biomarker analysis can be contextualized. The review of OCTA signal generation covers essential topics and is not exhaustive; for readers seeking more detailed accounts of similar material we recommend Kashani et al. [1] and Chen et al. [2]. We also note that, as a consequence of the large number of new OCTA studies published each year, OCTA terminology is sometimes unsettled or can change. We have tried to be consistent with accepted usage in this review, but researchers are encouraged to refer to Munk et al. [3] in their own work to avoid re-coining terms.

## 2. OCT angiography fundamentals

### 2.1. Flow signal generation in OCT angiography

Flow signal in OCTA data is generated by measuring intrinsic motion contrast between successive OCT cross-sectional scans (B-scans). Because it is an interferometric approach, the OCT signal includes both an amplitude and phase component. The flow signal can be generated by considering either of these channels independently (amplitude- or phase-based OCTA) or simultaneously

(complex-based OCTA). Phase must be compensated for in phase-based measurements [4]. Since amplitude measurements are sufficient to achieve capillary scale angiography, commercial manufacturers have mostly eschewed purely phase-based OCTA signal generation in favor of amplitude-based signal generation. Heidelberg, Optovue, and Topcon instruments all rely on amplitude-based processing. Complex-based OCTA uses all of the information collected from a cross-sectional scan, which is useful for improving flow detection sensitivity. Optical microangiography (OMAG) OCTA processing [5] does this in Zeiss instruments.

**Artificial intelligence-based flow signal generation.** Flow signal generation is also amenable to artificial intelligence-based methods [6]. Deep learning-based flow signal generation has at least one advantage relative to traditional signal processing approaches in that repeat scans to measure motion contrast are not strictly necessary; but in a study demonstrating flow signal generation from a single scan volume (i.e., a volume without repeats) angiograms lacked some capillary scale details that were apparent using traditional motion contrast approaches [7]. Flow signal generation from a single reflectance volume using artificial intelligence can be improved by considering vascular connectivity [8]. Artificial intelligence itself is a major area of active research in OCTA. For more information on this subject, readers are referred to Hormel et al. [9].

**Spectral splitting.** Motion contrast can be analyzed separately in different frequency bands and then averaged to produce a final estimate of magnitude [10]. This approach, “spectral splitting”, has been shown to improve flow detection sensitivity (or equivalently reduce the number of repeat scans needed to produce an adequate signal). The trade-off is loss of axial resolution: because each of the constituent frequency bands must be narrower than the full spectrum spectral splitting sacrifices axial resolution. Spectral divisions, however, can be chosen to maintain resolution sufficient to resolve capillaries. At a given resolution the number of spectral splits can be chosen to maximize flow signal-to-noise ratio [11]. Optovue devices use a spectral splitting algorithm, “split-spectrum amplitude-decorrelation” (SSADA) [10]. SSADA uses just the amplitude signal, but phase- and complex-based processing can also incorporate spectral splitting [12].

**Flow magnitude and interscan time.** For each of these approaches an important parameter is the inter-scan time between the successive B-scans. Even with erythrocyte density and vessel diameter being constant/consistent, flow signal is only linear for flow velocities within a certain range, the dynamic range, determined by the interscan time. [13–15]. Flow velocities that are above the dynamic range will lead to signal saturation in which OCTA becomes completely insensitive to differences in flow magnitude. Low flow velocities are even more problematic because vessels with low flow velocity, many of which are pathological, may not be detected at all. For this reason, the lack of flow signal in OCTA should not be mindlessly equated with a complete lack of flow. These constraints can lead to some trade-offs in the choice of interscan time for viewing different pathologies. For example, it has been suggested that the failure of OCTA to detect some microaneurysms is a result of interscan times being too short to register low flow speeds [16]. With at least three separate scans multiple interscan times can be sampled in order to extend the flow detection dynamic range and enable comparison of relative velocities. This approach, variable interscan time analysis (VISTA) [17], can help to characterize microaneurysms and other vascular disorders prevalent in diabetic retinopathy and other diseases [18–20]. Our group’s high dynamic range OCTA (HDR-OCTA) uses bidirectional scan patterns to extend the dynamic range more efficiently than raster scanning [21]. Both HDR-OCTA and VISTA can be helpful for blood flow velocity comparisons, but they are not necessary [22], and relative flow velocity estimation using eigenvalue decomposition has been verified using flow phantom experiments [23].

Blood flow velocity is not the only metric besides morphology that new approaches to OCTA measurement can interrogate. Flux is also important since it represents the amount of nutrient delivery achieved by blood flow more directly than flow velocity, which does not incorporate the blood volume moving through a region in a given time. OCTA proxies for flux have found

applications in explanatory studies of systemic disease [24], diabetic retinopathy [25], and glaucoma [26], among other pathologic features [27].

**Projection artifact removal.** In order to image deeper retinal and choroidal layers, the probe beam must traverse superficial tissue. If the superficial tissue includes vessels, time-varying shadows or multiply scattered photons can produce projection artifacts. These artifacts cause superficial vascular patterns to be mimicked in deeper layers. Projection artifact removal is a complicated problem. One way of removing projection artifacts is subtracting signal in *en face* images of more superficial layers from deeper [28–30], but this approach does not remove artifacts in cross-section and is prone to segmentation errors. It is best to compensate projection artifacts volumetrically so as to remove their influence in both *en face* and cross-sectional images; this can be done by considering the reflectance signal and signal attenuation in conjunction with the flow signal (Fig. 1) [31]. For a more detailed treatment of projection artifacts, readers are referred to Hormel et al. [32] and Spaide et al. [33]. For more information on projection-resolved OCTA readers can consult Hormel et al. [34].

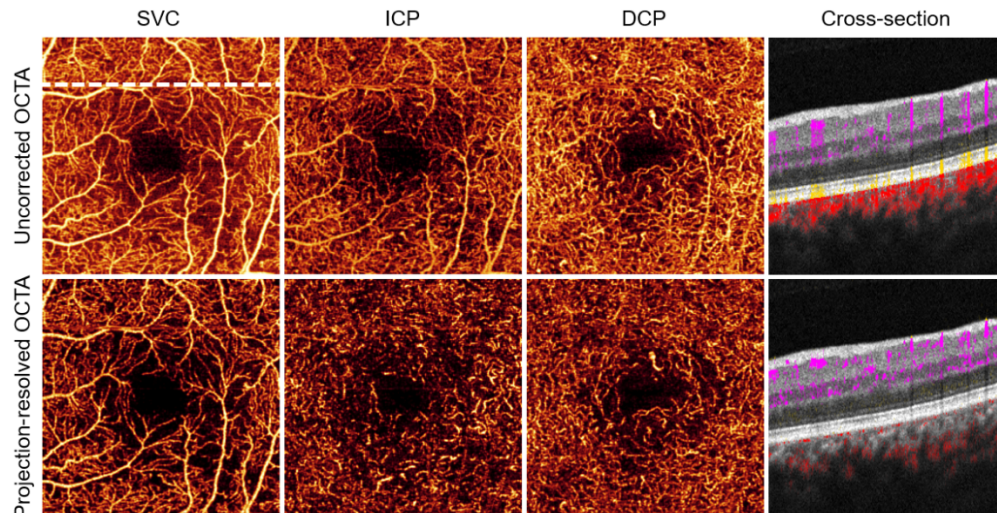


**Fig. 1. Projection artifact removal.** In the uncorrected angiograms (top row), projection artifacts in the *en face* images of the intermediate (ICP) and deep (DCP) capillary plexus show artefactual projection artifacts that mimic the pattern of large vessels in the superficial vascular complex (SVC). In cross-section at the location of the dotted line in the uncorrected SVC *en face* image, these artifacts appear as elongated tails underneath vessels, shown as flow signal (violet: inner retinal, yellow: outer retinal, red: choroidal) overlaid on the reflectance image. With permission from Wang et al. [31].

## 2.2. Angiogram construction

Once the flow signal has been generated, it still needs to be displayed for image graders and clinicians. Many algorithms also take angiogram images as input. Since the flow signal is captured in three dimensions, multiple data representations are possible. Volumetric displays are difficult to interpret. Most OCTA data is displayed in two dimensions, either in cross-section or *en face* representations. Cross-sectional images are useful for differentiating macular neovascularization lesion types [35,36] and identifying retinal neovascularization and related pathology [37,38]. *En face* images are useful because they display information analogously to color fundus photography and dye-based angiography, and because of the orientation of the retinal plexuses along the dimensions being viewed [39,40]. They can also be color-coded by depth in order to retain

volumetric information while retaining ease of interpretation [41]. *En face* angiograms can be constructed by projecting the flow signal through specific anatomic layers; using maximum value projection produces angiograms with higher flow signal-to-noise ratios and better repeatability than alternative projection methods [42,43].

Anatomic layer segmentation is needed to produce *en face* images. The retinal plexuses are located within or between different anatomic layers [39,40]. In addition to retinal vasculature, OCTA can also image the choriocapillaris. Furthermore, while OCTA cannot typically image deeper choroidal vessels, these can be visualized using the structural channel. To display any of these vascular tissues in isolation requires accurate segmentation of the boundaries between these layers. There are several approaches for segmenting retinal layer boundaries; for traditional rules-based algorithms graph search methods have been notably effective [44–46]. Like many image analysis problems, retinal layer segmentation can be addressed with deep learning algorithms [47,48]. Traditional and deep learning-based estimates of retinal layer boundaries can be refined by subsequent application of graph search methods [48,49]. And, while most layer segmentation methods rely on just the reflectance signal, the flow signal can also improve segmentation accuracy in some contexts, notably for the retinal pigment epithelium [50] and for identifying fluid regions [51].

Once an *en face* angiogram has been obtained, image quality can be improved through artifact reduction, filtering, and denoising. Scan misalignment due to involuntary eye movement can often be corrected by merging B-scans captured along orthogonal axes [52,53]. Image registration can also help to remove motion artifacts [54–56]. However, even with such approaches, some residual motion may manifest as flow signals in OCT angiograms, and signal attenuation or under-sampling can otherwise make vessels difficult to recognize. For this reason, vessels in *en face* images are frequently enhanced in software. Handcrafted vessel-enhancing filters have been applied to this purpose [57–59]. Deep learning has also been used to improve *en face* OCTA image quality, with deep learning networks capable of reconstructing under-sampled data volumes at improved resolution and signal-to-noise ratio (Fig. 2) [60,61]. Deep learning can also denoise angiograms volumetrically and in wide-field applications [62].

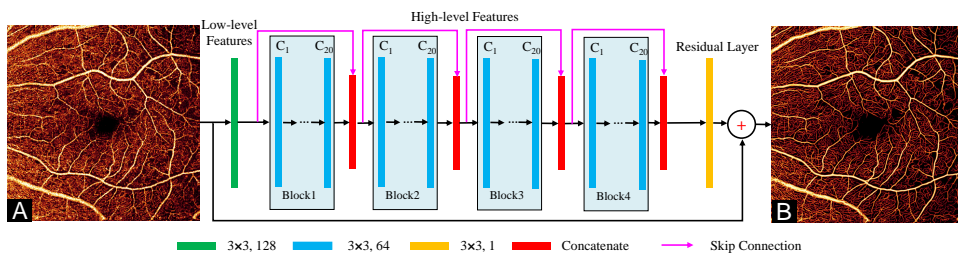


**Fig. 2. Angiogram reconstruction using deep learning.** The network is comprised of three parts: a low-level feature extraction layer, high-level feature extraction layers, and a residual layer. The kernel size in all the convolutional layers is  $3 \times 3$ . The number of channels in the green, blue, and yellow convolutional layer are 128, 64, and 1, respectively. Red layers are concatenation layers that concatenate the output of the convolution block with its input via skip connections. (A) Example input and (B) output 6  $\times$  6-mm angiogram. With permission from Gao et al. [61].

### 3. Imaging vascular biomarkers with OCT angiography

OCTA devices employing some innovations as described above are capable of imaging vascular morphology and pathology in human eyes with higher vascular contrast than alternatives such

as dye-based angiography [63,64], and in multiple layers [65]. In the following we discuss several of the biomarkers most often analyzed with OCTA. For readers seeking more information on the application of OCTA to disease in general, we recommend Spaide et al. as the most comprehensive review of the clinical applications of OCTA [66].

### 3.1. Perfusion

With its ability to detect blood flow in the retina and choriocapillaris, OCTA is useful for assessing perfusion. OCTA does not measure circulation directly due to the difficulty of accurately measuring flow velocity [13,15]; instead, OCTA measurements determine perfusion through proxy measurements that are ultimately different means of assessing vascular anatomy.

**Vessel density.** Vessel density (Fig. 3) is among the most common metrics assessed in OCTA images and is useful for staging and diagnosing prevalent diseases including age-related macular degeneration [67], diabetic retinopathy [68,69], and glaucoma [70–72]. It is usually measured as a percent area. However, given that the transverse resolution in commercial OCTA systems and most research instruments is lower than the anatomic width of capillaries, vessel density measured in this way is not anatomically correct. Obtaining anatomically correct vessel densities would require a reduced optical spot size on the retina relative to contemporary commercial devices as well as a sampling density similar to the scale of capillaries, ideally also meeting the Nyquist sampling criterion. This requirement becomes more arduous as fields of view in OCTA continue to expand due to the constitutive trade-off between field of view and sampling density for a scan acquired in a similar timeframe. Achieving high density sampling in large fields of view can significantly increase procedure times [73]. To avoid this issue, some vessel density measurements are made after vessel skeletonization.

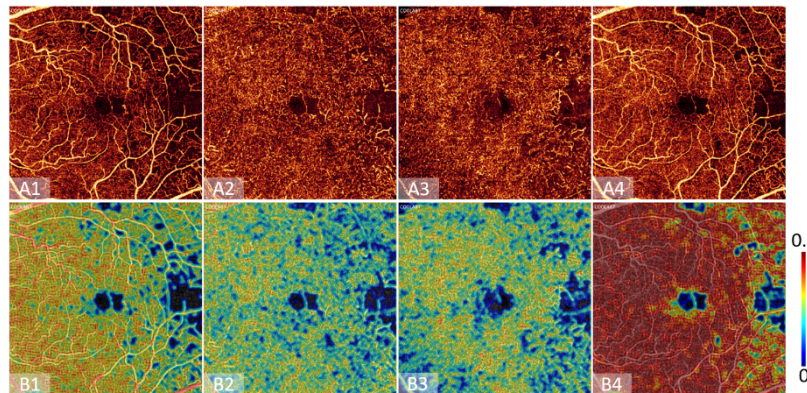


**Fig. 3. Vessel density maps in an eye with diabetic retinopathy.** Top row: projection-resolved angiograms of the superficial vascular complex (SVC; left), intermediate (ICP; middle) and deep (DCP; right) capillary plexuses. Second row: corresponding vessel density heatmaps from our group's COOL-ART reading software. The vessel density heatmaps reveal low vessel density in regions of capillary dropout.

A straightforward way to achieve a vessel density measurement is to segment vessels in *en face* images. Traditional methods mostly accomplish this through a combination of filtering and thresholding [68,74–76]; given that the background levels may vary throughout an image, it is worthwhile to perform compensation for variation in reflectance [77]. In addition to traditional, handcrafted thresholding methods, vessels can also be segmented with the aid of deep learning algorithms [60,61,78]. It should also be noted that many published results (e.g. [79–81]) rely on vessel density measurements supplied by commercial devices' proprietary software.

Direct comparison of the efficacy of most of these specific approaches is lacking. One study found that vessel density measurements based on deep learning were better able to stage glaucoma than traditional rules-based thresholding [78]. On the other hand, there does not seem to be a clear advantage for any traditional thresholding method compared to another in head-to-head comparisons [82]. While no traditional thresholding method is obviously superior to others, the choice of method can still lead to significant differences in vessel density measurements made on the same eye, as can the study instrument and scan location, pattern, and size [82–85]. If these confounding influences are accounted for, vessel density measurements achieve high repeatability [83,86,87]. In total, these conclusions indicate that when care is taken to preserve instrument type/flow signal generation, vessel segmentation approach, and scan parameters (pattern/location/size), vessel density measurements can be reliably compared, but not otherwise. Future comparisons between techniques could be facilitated by public datasets such as ROSE which enable direct comparisons [88].

Even though OCTA is a volumetric imaging modality, studies measuring vessel density in three-dimensions are rare. One study found that three-dimensional vessel density was more highly correlated with DR severity than two-dimensional, and also better able to diagnose different severities of the disease [89].

**Non-perfusion area.** Non-perfusion areas are localized regions of vessel loss and capillary drop-out. They are identified as regions in which the distance to the nearest vessel is larger than a physiologically determined threshold [90,91]. One subtlety is that since the distance to the nearest vessel in pathologic non-perfusion areas is often smaller than the foveal avascular zone, the foveal avascular zone is typically also segmented by non-perfusion area algorithms despite the fact that it is not pathological. Because the foveal avascular zone is large and highly variable in extent, it can adversely influence the utility of non-perfusion area measurements for disease diagnostics. To avoid this confounding influence, extrafoveal avascular area, measured only within regions beyond a set distance from the foveal avascular zone, is sometimes used as an alternative [91].

Strategies that rely on vessel segmentation to determine non-perfusion area are vulnerable to imaging artifacts such as signal attenuation (which can introduce false positive non-perfusion areas) or projection artifacts (which can introduce false negatives). Instead of measuring non-perfusion areas by segmenting vessels non-perfusion areas can be segmented directly using deep learning [92–94]. For this task it is useful to analyze the reflectance channel to identify projection [31] and signal reduction artifacts (Fig. 4) [95].

Non-perfusion area measurements are useful for assessing retinopathy severity [96,97]. For this purpose, it is also useful to measure non-perfusion area in individual plexuses since doing so can achieve better retinopathy staging, though some published studies disagree as to which plexus or complex is superior for this task [96,98]. These disparities may be the result of methodological differences in how non-perfused regions are detected.

**Choriocapillaris flow deficits.** Perfusion can also be lost in the choriocapillaris in several diseases, including leading causes of blindness such as AMD, DR, and glaucoma [99–103]. Imaging the choriocapillaris with OCTA is more difficult than imaging superficial retinal layers. The choriocapillaris is located beneath the retinal pigment epithelium, a strongly reflecting layer that attenuates the reflectance signal. Imaging in the choriocapillaris is consequently prone to both signal attenuation and projection artifacts, and the density of the choriocapillaris vasculature means that individual capillaries may not be resolvable. To ensure the challenges of imaging in this region are met it is important to consider the anatomic slab boundaries used, projection method employed, effect of scan size, sample beam wavelength, and comparisons to other imaging modalities for validation [104,105]. As with vessel density quantification, it is good practice to either preserve scan size or verify that measurements do not change between different scan patterns before comparison. And as noted above (**angiogram construction**), maximum projection seems

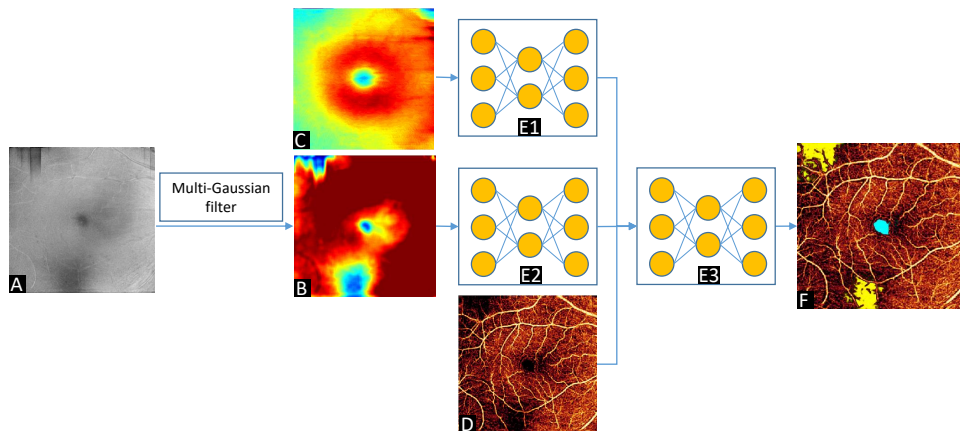


**Fig. 4. Non-perfusion area detection using deep learning.** (A) OCT reflectance image of the inner retina. (B) Gaussian-filtered reflectance intensity map of the inner retina. (C) Inner retinal thickness map. (D) The en face angiogram of the superficial vascular complex. (E1-E3) Three convolution networks with the same structure. (F) Detection result with probability maps for perfusion loss (blue) and signal reduction artifacts (yellow). With permission from Guo et al. [95].

to produce en face angiograms more amenable to quantification [42,43]. Because of its posterior location, signal penetration is essential for quality choriocapillaris imaging, and swept source devices that use longer wavelengths than spectral domain instruments (840 vs. 1050-nm) produce clearer choriocapillaris images due to longer wavelengths having superior tissue penetration [106,107]. Choriocapillaris boundary selection, however, is tricky. More superficial boundaries risk segmentation errors because the choriocapillaris is not always located a consistent depth from Bruch's membrane, but deeper boundaries may be visualizing projection artifacts and can be disrupted by *in situ* flow from deeper choroidal vessels [108,109].

In the choriocapillaris, due to anatomic differences with the retina, flow deficits are a better way to measure loss of perfusion than non-perfusion area. Similar to non-perfusion areas, flow deficits are regions that lack flow, but they are typically much smaller than non-perfusion areas. They are variously quantified as flow deficit percent area (which can be achieved across multiple scales), mean flow deficit area, flow deficit number, and total deficit area [19,110,111].

Since we need only know which pixels lack flow signal in order to identify flow deficits, we have another example of a vessel segmentation problem which can be solved using thresholding and filtering strategies similar to those used to measure vessel density. A popular approach is to use Phansalkar's method [112–115], but this approach is not necessarily superior to other choices such as fuzzy c-means depending on which flow deficit metric is being evaluated [111] (i.e. flow deficit density, total area, etc.). Complicating application of Phansalkar thresholding is the window radius parameter, which significantly affects flow deficit measurements; this parameter should be chosen to be between 1 and 2 times the (anatomic) vessel radius in the region of interest [111,116]. Another consideration for thresholding strategies for flow deficit detection is attenuation caused by concomitant pathology such as drusen, which can be both strong and localized. One method due to Zhang et al. compensated for this effect by multiplying the choriocapillaris angiogram by an inverted reflectance image of the same slab, thereby boosting the flow signal in areas of strong attenuation [110]. This approach was applied to multiple studies (e.g. [117–119]), but it can also introduce new artifacts which are exacerbated by projection artifact removal [109,120]. Restricting inverted reflectance values in hyporeflective regions can help alleviate this issue [121]. Regardless of the segmentation strategy used, it can also be helpful

to identify flow deficits that are larger than the average intercapillary spacing in order to assess pathology (Fig. 5) [111,119,122].

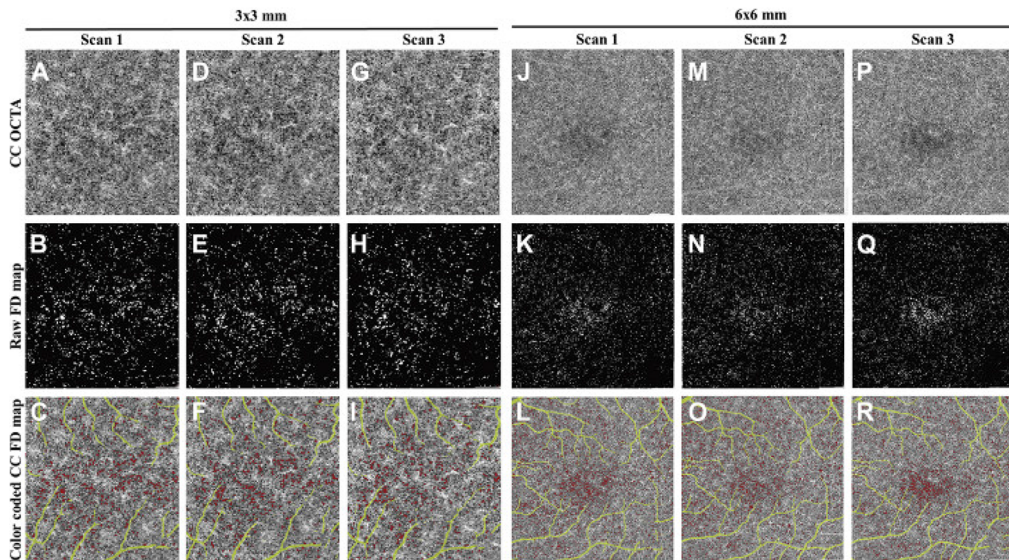


**Fig. 5. Choriocapillaris (CC) flow deficits identified with OCTA.** OCTA images were generated using 3 repeat  $3 \times 3$ - and  $6 \times 6$ -mm scans from a subject with normal eyes. (A, D, G, J, M, P) Swept source optical coherence tomography angiography (SS-OCTA) en face images. (B, E, H, K, N, Q) Binary images of segmented flow deficits (FDs) (white) using the fuzzy C-means method. (C, F, I, L, O, R) Color coded FD SS-OCTA map (red) after removing FDs below normal intercapillary distances and projection artifacts (yellow). Reprinted with permission from Chu et al. [111].

Flow deficit metrics are of particular use in analysis of AMD, where they can help with disease prognosis [112,123], are correlated with the presence of drusen [124] and neovascular lesions [125], and predict geographic atrophy lesion growth rate [117,126].

### 3.2. Foveal avascular zone metrics

The foveal avascular zone (FAZ) is enlarged and remodeled in several diseases [127–129]. It can be quantified with OCTA in order to gauge these developments using several metrics which could be divided into size and shape categories. For size, these would include FAZ area, horizontal and vertical diameter, and Feret diameter; for shape, circularity and aspect ratio (along other less common metrics for both) [130–133].

Measurement of the FAZ relies on accurately locating the surrounding vessels, so quantification relies on similar segmentation strategies as those discussed above for vessel density, non-perfusion, and choriocapillaris deficits (**Section: Perfusion**) measurements. Similar to vessel density measurements, published reports have noted high repeatability for FAZ metrics made on the same instrument using the same processing [134,135]. Amongst the metrics themselves, one study found that shape metrics obtain more repeatable measurements [133]. However, like vessel density measurements, FAZ statistics may yield significantly different results in the same eye imaged with different devices and segmentation approaches [85,136,137]. Deep learning has also been employed to segment the FAZ, with the result showing better agreement with manual segmentation in eyes with DR relative to a tradition rules-based method [138]. Deep learning methods have also been able to establish pre-clinical changes in the FAZ predictive of developing DR and loss of visual acuity [139].

An additional challenge for using the FAZ to diagnose and assess disease is the wide variation in FAZ area in healthy individuals [140]. Much more consistent is the width of the ganglion cell complex at the edge of the baseline FAZ (the original FAZ before the onset of DR) [141]. Vessel metrics within para-FAZ boundary region dictated by retinal thickness are better able to assess DR severity than the same metrics relying on the FAZ boundary dictated by the flow signal (Fig. 6) [89].

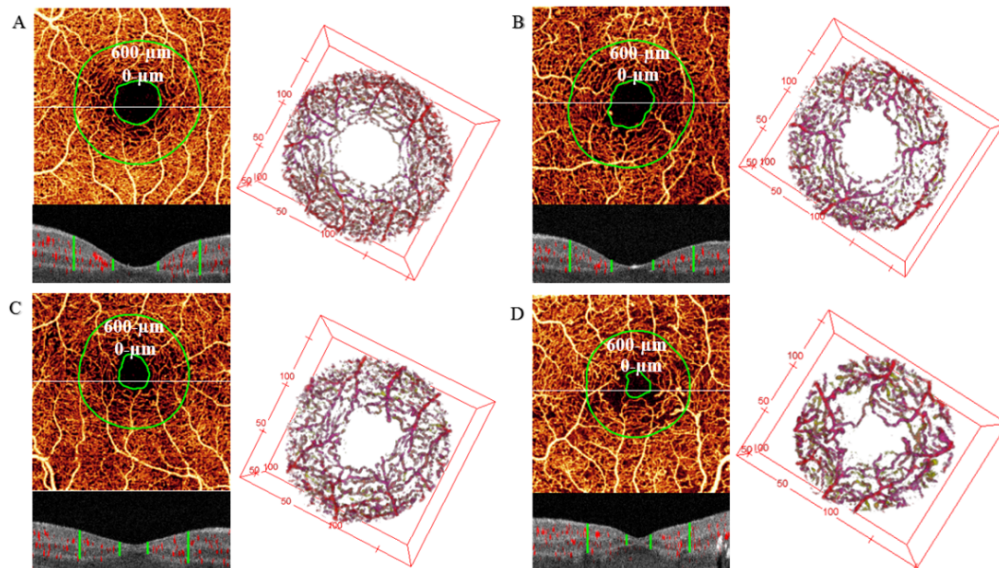


**Fig. 6.** Assessing perfusion loss near the foveal avascular zone (FAZ) using a baseline FAZ region determined from retinal thickness. 3D para-foveal avascular area (FAZ) vessel density in eyes of healthy control (A), diabetes without retinopathy (B), mild to moderate nonproliferative DR (NPDR) (C), and proliferative DR (PDR) (D). Upper panel of A-D: *en face* maximum projection of inner retinal angiogram. The inner green line represents the theoretical baseline FAZ (tbFAZ) boundary; the outer green line represents 600  $\mu\text{m}$  distances from the tbFAZ boundary in the transverse direction. The white horizontal line indicates the position of a representative B-scan in the panel below. Lower panel of A-D: cross-sectional B-scan overlaid with angiographic signal (red). The green vertical lines indicate the analytic para-FAZ volume boundary locations in the inner retina. Right panel of A-D: corresponding volumetric para-FAZ OCTA. With permission from Wang et al. [89].

### 3.3. Neovascularization

In the biomarkers already considered, pathology was largely indicated by a loss of vascularization. In neovascular lesions, the opposite occurs- new vessel growth creates pathology, which frequently leads to a serious threat to vision.

**Macular neovascularization.** Macular neovascularization (MNV) occurs in AMD, pathologic myopia, polypoidal choroidal vasculopathy, as well as rare diseases [142–145]. It is particularly important in AMD both because exudative AMD remains responsible for most cases of blindness [146], while at the same time neovascular AMD is treatable with anti-vascular endothelial growth factor (anti-VEGF) therapies [147]. Taken together, these facts mean that the detection of MNV is critical for preserving vision.

OCTA can differentiate between different MNV lesion types by locating them below (type I) or above (type II) retinal pigment epithelium or within the inner retina (type III) (Fig. 7) [9]. These lesion types may respond differently to treatment [148]. Lesion size and complexity, which are

both quantifiable with OCTA, are also predictive of treatment response [149,150]. Because it is non-invasive, OCTA is also a useful means for monitoring this response and lesion dynamics (Fig. 8) [151–153]. Because it is capable of detecting neovascular vessels before exudation has occurred, OCTA is also capable of analyzing pre-clinical lesions [154,155].

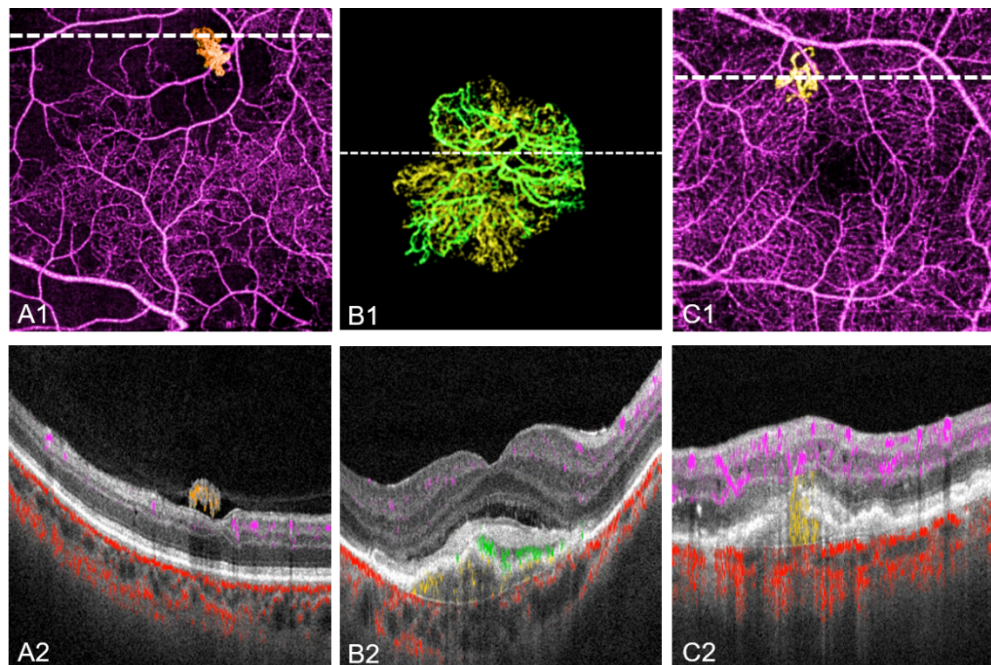


**Fig. 7. Differentiating neovascular lesion type with OCTA.** By overlaying the flow signal on the structural signal, a combination of structural OCT and OCTA is uniquely capable of ascertaining neovascular lesion type. Row 1: en face images; row 2: cross-sectional images taken at the location of the dotted white lines in row 1, with flow signal overlaid on the structural image. (A) Retinal neovascularization can be identified due to the location of the neovascular vessels above the internal limiting membrane. (B) A mixed type I / type II macular neovascular (MNV) lesion, with the type I component shown in yellow and the type II in green. The separate components can be identified by their location respectively below and above retinal pigment epithelium. (C) Type III MNV, with the cross-sectional image showing vessels extended between the choroid and retina. With permission from Hormel et al. [9].

MNV lesion and vessel area and are both amenable to automated quantification in OCTA. However, MNV often occurs in the outer retina, which is one of the more difficult regions to visualize using OCTA due to the nearby presence of the highly reflecting RPE, which produces strong projection artifacts. Deep learning in combination with a well-chosen set of image inputs is able to distinguish these projection artifacts, and is capable of accurately segmenting both MNV lesions and vasculature [157]. A deep-learning-based approach was recently demonstrated to be capable of identifying MNV lesions in a large, clinically-realistic dataset including several diseases with MNV and multiple images of healthy eyes and eyes with diseases (including less advanced stages of AMD) without [156].

**Retinal neovascularization.** Unlike MNV, retinal neovascularization (RNV) can occur throughout the retina, including in peripheral regions far from the macula [158]. It is a key pathologic development and treatment indicator in ischemic retinopathies, notably for DR and

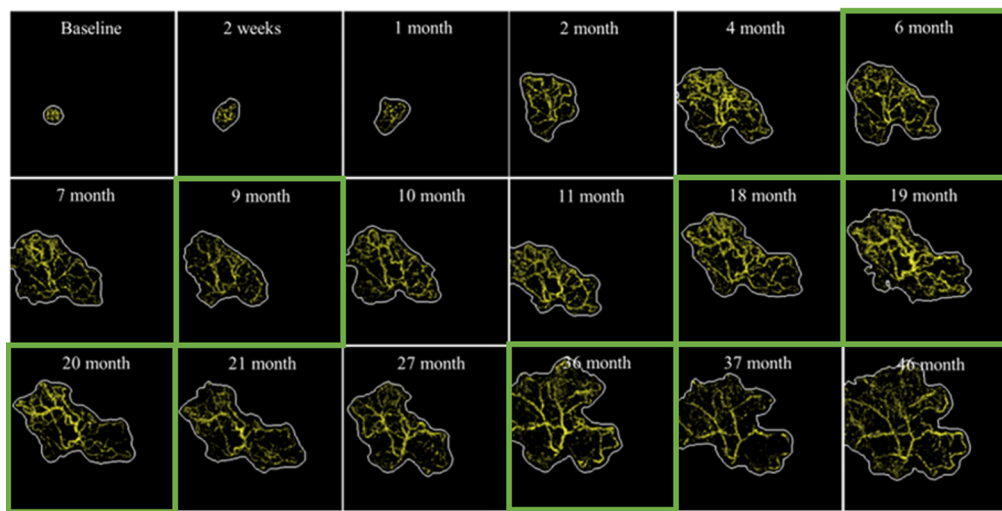


**Fig. 8. Macular neovascularization (MNV) treatment response imaged by OCTA.** En face images show the lesion at baseline and up to 46 months of follow up, with green borders indicating visits in which anti-VEGF therapy was administered. Anti-VEGF treatments were also provided on months 25 and 33, which are not shown above. With permission from Wang et al. [156].

retinopathy of prematurity (ROP) [159,160]. Similar to MNV, RNV can lead to vision loss while also being treatable with anti-VEGF therapy [161]. Detecting RNV is therefore a clinical priority.

Peripheral lesions remain the most challenging aspect of characterizing RNV with OCTA due to the small fields of view in contemporary commercial devices. For this reason ultrawide-field OCTA is advantageous for detecting RNV [37]. With OCTA RNV can be easily identified by its location anterior to the inner limiting membrane (Fig. 7) [27,162,163]. As a result, In head-to-head comparisons across the same field of view OCTA achieves equivalent or superior detection sensitivity relative to fluorescein angiography and color fundus photography [37,158].

OCTA is advantageous for RNV analysis beyond just detection sensitivity. Similar to MNV, OCTA can be used to monitor treatment response [164]. Another advantage for OCTA imaging is that structural OCT data can be generated alongside the flow signal from data accrued during the same procedure. Presumed glial sprouts visible in the structural channel may be precursors to RNV [38]; observation of a combination of these features enabled detection of clinically unsuspected RNV [162]. The structural channel is additionally useful for distinguishing RNV from intraretinal microvascular abnormalities (IRMA) [165].

### 3.4. Vasculopathies

OCTA can also image pathology that directly affects vessels. The effective analytic methods on these vasculopathy features would be very helpful for comprehensively investigating them.

**Collateral vessels.** Collateral vessels are one of several features relevant to branch retinal vein occlusion visible with OCTA (Fig. 9) [166–168]. OCTA identifies more collateral vessels than fluorescein angiography [169]. OCTA-based studies support the conclusion that collateral vessels form in the deep capillary plexus as a result of capillary dropout [168,170].

**Intraretinal microvascular abnormalities.** Intraretinal microvascular abnormalities (IRMA) are a pathologic feature in DR defined by the Early Treatment of Diabetic Retinopathy Study Group as tortuous vessels exhibiting dilation [171]. OCTA is useful for imaging IRMA for two reasons. First, it has a higher IRMA detection sensitivity than fundus photography, the other

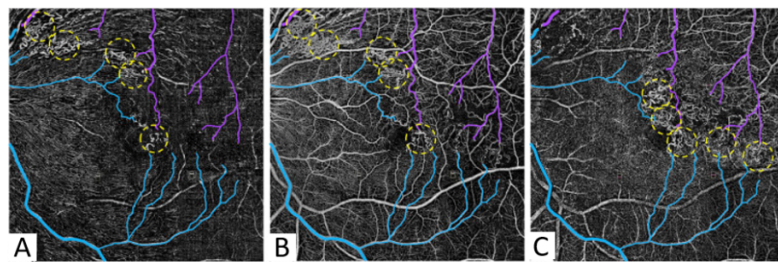


**Fig. 9.** Collateral vessels imaged with OCTA. (A) Radial peripapillary capillary plexus, (B) superficial vascular complex, and (C) deep capillary plexus. Normal veins are blue, and affected veins are purple. Yellow dashed circle in each layer indicates the collateral vessels, defined as dilated capillaries between the normal and affected veins. With permission from Tsuboi et al. [168].

major screening modality for DR [172]. Second, OCTA combined with structural OCT can distinguish between IRMA and RNV, as a flow overlay on reflectance cross-sectional images can clearly determine if flow is present above the inner limiting membrane [165]. In *en face* OCTA, IRMA is characterized by tortuous, dilated capillary loops [173]. This appearance, along with associated non-perfusion area, can be monitored to evaluate treatment response [173].

**Microaneurysms.** Microaneurysms are capillary dilations with multiple morphologies usually occurring in the deep capillary plexus [174,175]. They are an important pathologic feature in DR, where they are often the first pathology to develop [176].

The gold standard for microaneurysm detection remains dye-based angiography. Microaneurysms can occur throughout the retina, and the larger fields of view attainable by commercial dye-based angiography imaging is beneficial for identifying peripheral microaneurysms. While microaneurysms are visible with OCTA [177], multiple studies have demonstrated that even within the same field of view dye-based angiography achieves a higher microaneurysm detection sensitivity than OCTA [178–181], through it should be noted that some microaneurysms visible with OCTA may not be detected with dye-based angiography [182], and furthermore some features that appear to be microaneurysms with dye-based angiography can be recognized as small neovascular lesions using OCTA [163]. Multiple *en face* image averaging in OCTA can improve microaneurysm detection sensitivity [179].

The appearance of microaneurysms in OCTA recapitulates findings from histology, with focal bulging, fusiform, and saccular types all visible [183]. Additional types identified in OCTA are “pedunculated” and “irregular” [183]. OCTA can reach beyond just the flow signal characteristics in order to identify further types of microaneurysms based on their appearance in the structural OCT channel [182] (Fig. 10). These characterizations include the reflectivity of the associated tissue, with hyper-reflective microaneurysms more associated with fluid accumulation than hypo-reflective [184,185]. Some microaneurysms lack flow signal altogether; microaneurysms with flow signal present are more closely associated with retinal fluid than those without [182].

**Venous beading.** Venous beading is used by the Early Treatment of Diabetic Retinopathy Study (ETDRS) scale to stage DR [171]. Venous beading is visible with OCTA [131,186,187], and OCTA was also able to determine that flow speed in affected veins is relatively high [18].

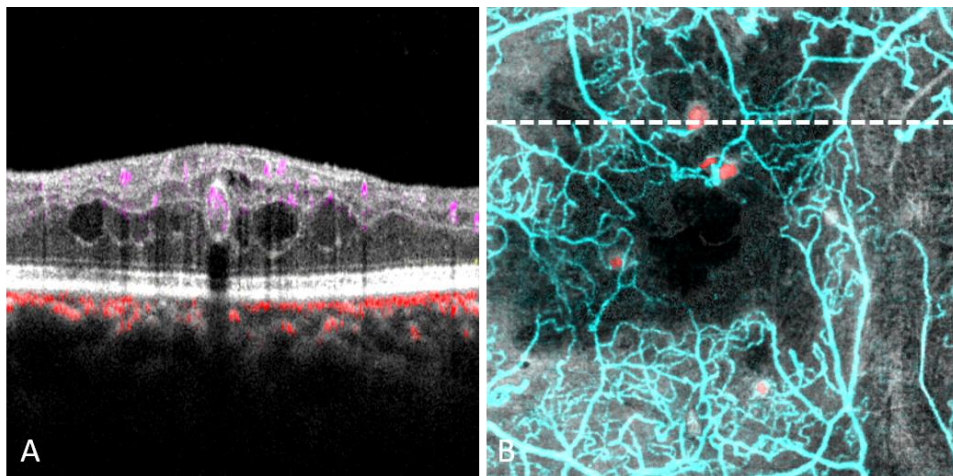


**Fig. 10. Microaneurysms characterization using OCTA.** While dye-based angiography has a superior detection sensitivity, OCTA do more than simply identify microaneurysms. (A) Flow signal (retinal: violet, choroidal: red) overlaid on a structural cross-sectional scan. The microaneurysm is apparent in the structural channel as a hyper-reflective oval. (B) En face image, with the location of the cross-sectional scan in (A) marked by a dotted white line. Arrows indicate microaneurysms identified on cross-sectional scans in which flow is either present (red) or absent (blue). Microaneurysms with flow signal present are more likely to be associated with retinal fluid than those without, indicating a relevant physiological difference between the microaneurysm types. With permission from Gao et al. [182].

#### 4. Future directions

OCTA can image most vascular pathology identifiable with alternative imaging modalities, and in many cases offers improved detection sensitivity, clearer images, and additional information such as the full three-dimensional location of pathology. Nonetheless some aspects of OCTA imaging remain to be improved in order to enable better characterization of pathologic features relevant to disease.

**Field of view.** OCTA can provide improved detection sensitivity for several biomarkers relative to fundus photography and fluorescein angiography covering a similar field of view [37,98]. However, both these alternative imaging modalities can provide much larger fields of view than contemporary commercial OCTA devices. This means, for example, that while OCTA can provide superior staging of DR from non-perfusion area within an equivalent field of view compared to fluorescein angiography, ultrawide-field fluorescein angiography may still achieve slightly higher diagnostic accuracy [98]. This implies that extending the field of view in OCTA imaging could lead to improved characterization of the biomarkers discussed in this work which could in turn lead to improved OCTA based diagnosis. In fact this has been demonstrated for non-perfusion area in DR diagnostics (Fig. 11) [188]. However, it should be noted that enlarged fields of view can exacerbate signal reduction artifacts due to sources like vignetting and optical aberrations, which could in turn cause false positive non-perfusion area identification; it is therefore important to review wide-field scans in order to identify regions affected signal reduction when measuring non-perfusion areas [189]. Data-driven image denoising could also help with this issue and possibly identification of other peripheral pathologic features [60–62]. Detection of treatment indicators such as retinal neovascularization in enlarged fields of view would deliver immense benefit to clinical practice [37]. With the development of swept-source

systems, contemporary research devices can obtain 75-degree fields of view in a single shot [190] or larger 90-degree fields of view with montage [62].

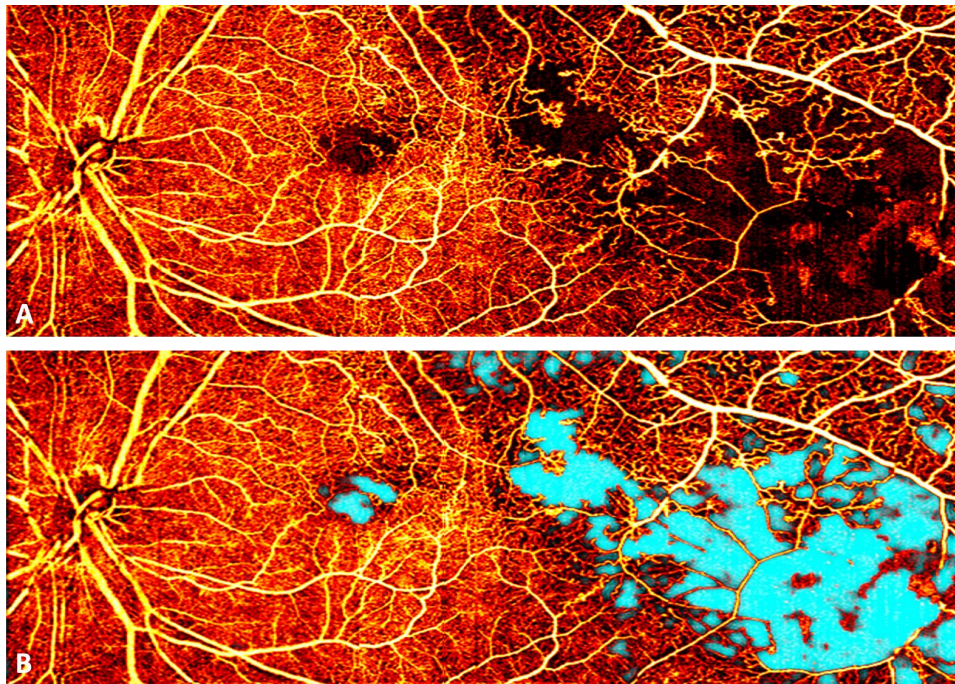


**Fig. 11. Non-perfusion area segmentation using artificial intelligence in a montaged widefield scan.** (A) Wide-field angiogram including the macula, optic disc, and temporal retina; (B) network output, with non-perfusion area labeled in teal and brightness indicating network prediction confidence. Enlarging the field of view can improve diagnostic accuracy for staging diabetic retinopathy based on non-perfusion area. With permission from Guo et al. [95].

**Quantification.** Many of the pathologic features discussed here, including vessel density, non-perfusion area, flow deficits, foveal avascular zone metrics, and macular neovascularization, can be quantified using OCTA. Others, such as venous beading, remain at an observational stage in OCTA analysis. The ability to quantify features vastly improves our ability to use them to stage and diagnose disease, as well as evaluate treatment efficacy and response. Pathologic features that currently lack tools for quantification would benefit from having such tools developed, but some new quantification approaches may need to rely on advanced image processing such as deep learning in order to achieve adequate performance. For example, to identify venous beading it would be useful to be able to differentiate arteries and veins. This is a difficult task to perform even for trained graders, but deep-learning-based algorithms can perform differentiate arteries and veins directly from just OCTA data (Fig. 12) [191,192].

**Correlation with other pathologic features and function.** OCTA biomarkers are morphological, and so do not directly assess visual or cellular function. OCTA is obviously most easily correlated with structural OCT data because they can be captured from the same procedure and the structural/vascular information from these sources is automatically co-registered. This registration allows for excellent measurements of correlations between vascular and structural pathologies images with OCT/OCTA devices, such as the relationship between microaneurysms and retinal fluid noted above [182]. Other imaging modalities can also supplement OCTA, for example in one study where adaptive optics scanning laser ophthalmoscopy was able to image cellular-scale

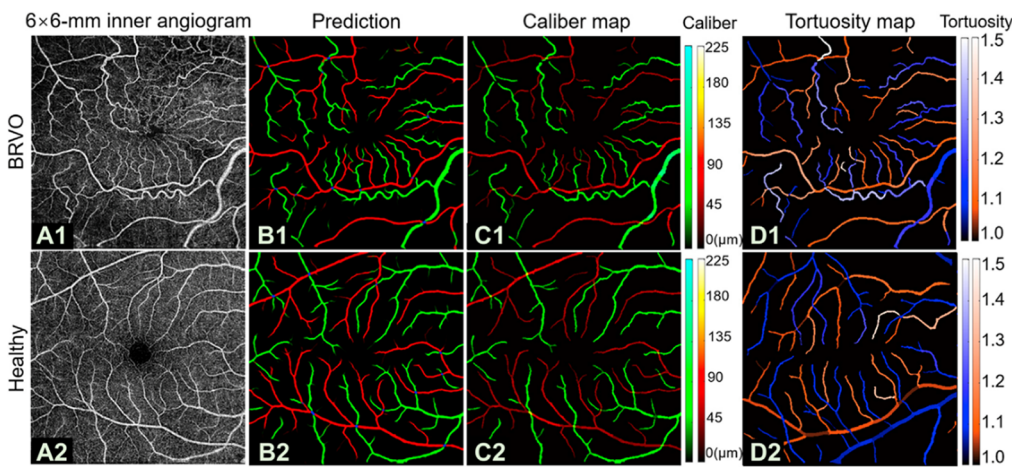


**Fig. 12. Artery/vein differentiation in OCTA using deep learning.** Row 1: an eye with branch retinal vein occlusion (BRVO); row 2: a healthy eye. (A) 6 × 6-mm inner retinal macular scans. (B) The output of a deep learning network trained to identify arteries (red) and veins (green). Differentiating vessel type allows common vessel metrics such as caliber (C) and tortuosity (D) to be quantified separately in arteries and veins. These separate quantifications could be useful in assessing diseases that affect arteries and veins differently, such as in BRVO. Artery/vein identification could also be a useful step for quantifying biomarkers such as venous beading. Adapted with permission from Gao et al. [191].

abnormalities in ischemic regions identified with OCTA [193]. This approach has the potential to elucidate disease mechanisms by compiling synergistic information that would not be available from just OCTA measurements of vascular pathology. Similarly, direct comparisons between OCTA and function must rely on other imaging modalities. For example, OCTA measurements correlation with microperimetry measurements of visual field in glaucoma [194,195]. One very promising avenue of research in this respect is OCT-based optoretinography [196–198], which uses high-resolution OCT imaging to quantify retinal response to photostimulation and, similar to structural OCT, could be automatically co-registered with vascular information for OCTA in order to explore the relationship between vascular structure and function.

**Biomarker-free diagnostics.** As an alternative to any of the biomarkers discussed here, advanced algorithms can diagnose disease directly from images, without appeal to any specific features. Indeed, Eyenuk provided the first example of an automated image diagnostic platform to gain FDA approval, and is used to diagnose DR. Several published results indicate that OCTA scans can be analyzed directly by deep learning networks in order to provide diagnosis [199–204]. All of these approaches remain to be scaled in order to be applied to clinical practice. Through the use of interpretability tools such as class activation maps could these networks could also help identify new biomarkers that could subsequently be investigated and, eventually, reviewed in an update to this work [205].

One additional shortcoming for OCTA studies concerns not the imaging technology itself, but rather its maturity (or lack thereof): most OCTA studies are cross-sectional, in part simply because the technology has not been around long enough to accrue many longitudinal results. Future longitudinal could reveal new uses for the biomarkers discussed here and improve their efficacy for evaluating disease and treatment options.

## 5. Conclusion

By providing high-resolution, depth-resolved images of retinal and choroidal vasculature non-invasively, OCTA can improve clinical practice and therapeutic research. OCTA images are amenable to quantification, and measurement of biomarkers can inform research and improve clinical practice. The amount of detail available in OCTA data is beneficial for characterizing biomarkers, and as we develop better tools for this purpose we can expect a deeper understanding of their role in disease to develop as well.

**Funding.** BrightFocus Foundation (G2020168, M20230081); Edward N. and Della L. Thome Memorial Foundation; Research to Prevent Blindness (Unrestricted departmental fund; Dr. H. James and Carole Free Catalyst Award); Malcolm M. Marquis, MD Endowed Fund for Innovation; National Institutes of Health (P30 EY010572, R01 EY023285, R01 EY024544, R01 EY027833, R01 EY031394, R01 EY035410, T32 EY023211, UL1TR002369).

**Disclosures.** Yali Jia: Optovue/Visionix, Inc. (P, R), Optos (P). The potential conflicts of interest have been reviewed and managed by OHSU. Other authors declare no conflicts of interest related to this article.

**Data availability.** Data underlying the results presented in this paper are not publicly available at this time but may be obtained from the authors upon reasonable request.

## References

1. A. H. Kashani, C. L. Chen, J. K. Gahm, F. Zheng, G. M. Richter, P. J. Rosenfeld, Y. Shi, and R. K. Wang, "Optical coherence tomography angiography: A comprehensive review of current methods and clinical applications," *Prog. Retin. Eye Res.* **60**, 66–100 (2017).
2. C.-L. Chen and R. K. Wang, "Optical coherence tomography based angiography [Invited]," *Biomed. Opt. Express* **8**(2), 1056–1082 (2017).
3. M. R. Munk, A. H. Kashani, and R. Tadayoni, *et al.*, "Recommendations for OCT angiography reporting in retinal vascular disease: a Delphi approach by international experts," *Ophthalmol. Retin.* **6**(9), 753–761 (2022).
4. M. Szkulmowski, I. Grulkowski, D. Szlag, A. Szkulmowska, A. Kowalczyk, and M. Wojtkowski, "Flow velocity estimation by complex ambiguity free joint spectral and time domain optical coherence tomography," *Opt. Express* **17**(16), 14281–14297 (2009).
5. L. An, T. T. Shen, and R. K. Wang, "Using ultrahigh sensitive optical microangiography to achieve comprehensive depth resolved microvasculature mapping for human retina," *J. Biomed. Opt.* **16**(10), 106013 (2011).
6. Z. Jiang, Z. Huang, B. Qiu, X. Meng, Y. You, X. Liu, G. Liu, C. Zhou, K. Yang, A. Maier, Q. Ren, and Y. Lu, "Comparative study of deep learning models for optical coherence tomography angiography," *Biomed. Opt. Express* **11**(3), 1580 (2020).
7. C. S. Lee, A. J. Tyring, Y. Wu, S. Xiao, A. S. Rokem, N. P. DeRuyter, Q. Zhang, A. Tufail, R. K. Wang, and A. Y. Lee, "Generating retinal flow maps from structural optical coherence tomography with artificial intelligence," *Sci. Rep.* **9**(1), 5694 (2019).
8. D. Le, T. Son, T.-H. Kim, M. Abtahi, T. Adejumo, and X. Yao, "Retinal vascular connectivity network for deep learning OCTA construction from single OCT volume scan," *Proc. SPIE* **12360**, 1236003 (2023).
9. T. T. Hormel, T. S. Hwang, S. T. Bailey, D. J. Wilson, D. Huang, and Y. Jia, "Artificial intelligence in OCT angiography," *Prog. Retin. Eye Res.* **85**, 100965 (2021).
10. Y. Jia, O. Tan, J. Tokayer, B. Potsaid, Y. Wang, J. J. Liu, M. F. Kraus, H. Subhash, J. G. Fujimoto, J. Horngger, and D. Huang, "Split-spectrum amplitude-decorrelation angiography with optical coherence tomography," *Opt. Express* **20**(4), 4710–4725 (2012).
11. S. S. Gao, G. Liu, D. Huang, and Y. Jia, "Optimization of the split-spectrum amplitude-decorrelation angiography algorithm on a spectral optical coherence tomography system," *Opt. Lett.* **40**(10), 2305–2308 (2015).
12. G. Liu, Y. Jia, A. D. Pechauer, R. Chandwani, and D. Huang, "Split-spectrum phase-gradient optical coherence tomography angiography," *Biomed. Opt. Express* **7**(8), 2943–2954 (2016).
13. J. P. Su, R. Chandwani, S. S. Gao, A. D. Pechauer, M. Zhang, J. Wang, Y. Jia, D. Huang, and G. Liu, "Calibration of optical coherence tomography angiography with a microfluidic chip," *J. Biomed. Opt.* **21**(08), 086015 (2016).
14. J. Tokayer, Y. Jia, A.-H. Dhalla, and D. Huang, "Blood flow velocity quantification using split-spectrum amplitude-decorrelation angiography with optical coherence tomography," *Biomed. Opt. Express* **4**(10), 1909 (2013).
15. W. J. Choi, W. Qin, C.-L. Chen, J. Wang, Q. Zhang, X. Yang, B. Z. Gao, and R. K. Wang, "Characterizing relationship between optical microangiography signals and capillary flow using microfluidic channels," *Biomed. Opt. Express* **7**(7), 2709 (2016).
16. S. Nakao, S. Yoshida, Y. Kaizu, M. Yamaguchi, I. Wada, T. Ishibashi, and K. hei Sonoda, "Microaneurysm detection in diabetic retinopathy using OCT angiography may depend on intramicroaneurysmal turbulence," *Ophthalmol. Retin.* **2**(11), 1171–1173 (2018).
17. S. B. Ploner, E. M. Moulton, W. Choi, N. K. Waheed, B. Lee, E. A. Novais, E. D. Cole, B. Potsaid, L. Husvogt, J. Schottenhamml, A. Maier, P. J. Rosenfeld, J. S. Duker, J. Horngger, and J. G. Fujimoto, "Toward quantitative optical coherence tomography angiography: Visualizing blood flow speeds in ocular Pathology using variable interscan time analysis," *Retina* **36**(Supplement 1), S118–S126 (2016).

18. M. Arya, M. B. Filho, C. B. Rebhun, E. M. Moult, B. Lee, Y. Alibhai, A. J. Witkin, C. R. Baumal, J. S. Duker, J. G. Fujimoto, and N. K. Waheed, "Analyzing relative flow speeds in diabetic retinopathy using variable interscan time analysis OCT angiography," *Ophthalmol. Retin.* **5**(1), 49–59 (2021).
19. E. M. Moult, A. Y. Alibhai, B. K. Lee, Y. Yu, S. Ploner, S. Chen, A. Maier, J. S. Duker, N. K. Waheed, and J. G. Fujimoto, "A framework for multiscale quantitation of relationships between choriocapillaris flow impairment and geographic atrophy growth," *Am. J. Ophthalmol.* **214**, 172–187 (2020).
20. C. B. Rebhun, E. M. Moult, E. A. Novais, C. Moreira-Neto, S. B. Ploner, R. N. Louzada, B. Lee, C. R. Baumal, J. G. Fujimoto, J. S. Duker, N. K. Waheed, and D. Ferrara, "Polypoidal choroidal vasculopathy on swept-source optical coherence tomography angiography with variable interscan time analysis," *Trans. Vis. Sci. Technol.* **6**(6), 4 (2017).
21. X. Wei, T. T. Hormel, S. Pi, Y. Guo, Y. Jian, and Y. Jia, "High dynamic range optical coherence tomography angiography (HDR-OCTA)," *Biomed. Opt. Express* **10**(7), 3560 (2019).
22. D. Richter, A. M. Fard, J. Straub, W. Wei, Q. Zhang, and R. K. Wang, "Relative retinal flow velocity detection using optical coherence tomography angiography imaging," *Biomed. Opt. Express* **11**(11), 6710 (2020).
23. R. K. Wang, Q. Zhang, Y. Li, and S. Song, "Optical coherence tomography angiography-based capillary velocimetry," *J. Biomed. Opt.* **22**(6), 066008 (2017).
24. S. Kushner-Lenho, Y. Li, Q. Zhang, R. K. Wang, X. Jiang, and A. H. Kashani, "OCTA derived vessel skeleton density versus flux and their associations with systemic determinants of health," *Invest. Ophthalmol. Visual Sci.* **63**(2), 19 (2022).
25. A. K. Dadzie, D. Le, M. Abtahi, B. Ebrahimi, T. Son, and I. Jennifer, "Normalized blood flow index in optical coherence tomography angiography provides a sensitive biomarker of early diabetic retinopathy," *Trans. Vis. Sci. Technol.* **12**(4), 3 (2023).
26. Y. Jia, E. Wei, X. Wang, X. Zhang, J. C. Morrison, M. Parikh, L. H. Lombardi, D. M. Gatley, R. L. Armour, B. Edmunds, M. F. Kraus, J. G. Fujimoto, and D. Huang, "Optical coherence tomography angiography of optic disc perfusion in glaucoma," *Ophthalmology* **121**(7), 1322–1332 (2014).
27. Y. Jia, S. T. Bailey, T. S. Hwang, S. M. McClintic, S. S. Gao, M. E. Pennesi, C. J. Flaxel, A. K. Lauer, D. J. Wilson, J. Horng, J. G. Fujimoto, and D. Huang, "Quantitative optical coherence tomography angiography of vascular abnormalities in the living human eye," *Proc. Natl. Acad. Sci. U. S. A.* **112**(18), E2395–E2402 (2015).
28. Y. Jia, S. T. Bailey, D. J. Wilson, O. Tan, M. L. Klein, C. J. Flaxel, B. Potsaid, J. J. Liu, C. D. Lu, M. F. Kraus, J. G. Fujimoto, and D. Huang, "Quantitative optical coherence tomography angiography of choroidal neovascularization in age-related macular degeneration," *Ophthalmology* **121**(7), 1435–1444 (2014).
29. A. Zhang, Q. Zhang, and R. K. Wang, "Minimizing projection artifacts for accurate presentation of choroidal neovascularization in OCT micro-angiography," *Biomed. Opt. Express* **6**(10), 4130–4143 (2015).
30. Q. Zhang, A. Zhang, C. S. Lee, A. Y. Lee, K. A. Rezaei, L. Roisman, A. Miller, F. Zheng, G. G. Gregori, M. K. Durbin, L. An, P. F. Stetson, P. J. Rosenfeld, and R. K. Wang, "Projection artifact removal improves visualization and quantitation of macular neovascularization imaged by optical coherence tomography angiography," *Ophthalmol. Retin.* **1**(2), 124–136 (2017).
31. J. Wang, T. T. Hormel, S. T. Bailey, T. S. Hwang, D. Huang, and Y. Jia, "Signal attenuation-compensated projection-resolved OCT angiography," *Biomed. Opt. Express* **14**(5), 2040–2054 (2023).
32. T. T. Hormel, D. Huang, and Y. Jia, "Artifacts and artifact removal in optical coherence tomographic angiography," *Quant. Imaging Med. Surg.* **11**(3), 1120–1133 (2020).
33. R. F. Spaide, J. G. Fujimoto, and N. K. Waheed, "Image artifacts in optical coherence angiography," *Retina* **35**, 2163 (2015).
34. T. T. Hormel, Y. Jia, Y. Jian, T. S. Hwang, S. T. Bailey, M. E. Pennesi, D. J. Wilson, J. C. Morrison, and D. Huang, "Plexus-specific retinal vascular anatomy and pathologies as seen by projection-resolved optical coherence tomographic angiography," *Prog. Retin. Eye Res.* **80**, 100878 (2020).
35. K. V. Bhavsar, Y. Jia, J. Wang, R. C. Patel, A. K. Lauer, D. Huang, and S. T. Bailey, "Projection-resolved optical coherence tomography angiography exhibiting early flow prior to clinically observed retinal angiomatic proliferation," *Am. J. Ophthalmol. Case Reports* **8**, 53–57 (2017).
36. A. Faridi, Y. Jia, S. S. Gao, D. Huang, K. V. Bhavsar, D. J. Wilson, A. Sill, C. J. Flaxel, T. S. Hwang, A. K. Lauer, and S. T. Bailey, "Sensitivity and specificity of OCT angiography to detect choroidal neovascularization," *Ophthalmol. Retin.* **1**(4), 294–303 (2017).
37. Q. S. You, Y. Guo, J. Wang, X. Wei, A. Camino, P. Zang, C. J. Flaxel, S. T. Bailey, D. Huang, Y. Jia, and T. S. Hwang, "Detection of clinically unsuspected retinal neovascularization with wide-field optical coherence tomography angiography," *Retina* **40**(5), 891–897 (2020).
38. K. Tsuboi, Y. Ishida, T. Wakabayashi, and M. Kamei, "Presumed glial sprouts as a predictor of preretinal neovascularization in retinal vein occlusion," *JAMA Ophthalmol.* **140**(3), 284–285 (2022).
39. J. P. Campbell, M. Zhang, T. S. Hwang, S. T. Bailey, D. J. Wilson, Y. Jia, and D. Huang, "Detailed vascular anatomy of the human retina by projection-resolved optical coherence tomography angiography," *Sci. Rep.* **7**(1), 42201 (2017).
40. P. L. Nesper and A. A. Fawzi, "Human parafoveal capillary vascular anatomy and connectivity revealed by optical coherence tomography angiography," *Invest. Ophthalmol. Visual Sci.* **59**(10), 3858–3867 (2018).
41. R. K. Wang, L. An, P. Francis, and D. J. Wilson, "Depth-resolved imaging of capillary networks in retina and choroid using ultrahigh sensitive optical microangiography," *Opt. Lett.* **35**(9), 1467 (2010).

42. T. T. Hormel, J. Wang, S. T. Bailey, T. S. Hwang, D. Huang, and Y. Jia, "Maximum value projection produces better en face OCT angiograms than mean value projection," *Biomed. Opt. Express* **9**(12), 6412–6424 (2018).
43. I. Byon, A. R. Alagorie, Y. Ji, L. Su, and S. R. Sadda, "Optimizing the repeatability of choriocapillaris flow deficit measurement from optical coherence tomography angiography," *Am. J. Ophthalmol.* **219**, 21–32 (2020).
44. B. J. Antony, M. D. Abràmoff, K. Lee, P. Sonkova, P. Gupta, Y. Kwon, M. Niemeijer, Z. Hu, and M. K. Garvin, "Automated 3D segmentation of intraretinal layers from optic nerve head optical coherence tomography images," *Proc. SPIE* **7626**, 76260U (2010).
45. S. J. Chiu, X. T. Li, P. Nicholas, C. A. Toth, J. A. Izatt, and S. Farsiu, "Automatic segmentation of seven retinal layers in SDOCT images congruent with expert manual segmentation," *Opt. Express* **18**(18), 19413–19428 (2010).
46. Y. Guo, A. Camino, M. Zhang, J. Wang, D. Huang, T. Hwang, and Y. Jia, "Automated segmentation of retinal layer boundaries and capillary plexuses in wide-field optical coherence tomographic angiography," *Biomed. Opt. Express* **9**(9), 4429–4442 (2018).
47. L. Fang, D. Cunefare, C. Wang, R. H. Guymer, S. Li, and S. Farsiu, "Automatic segmentation of nine retinal layer boundaries in OCT images of non-exudative AMD patients using deep learning and graph search," *Biomed. Opt. Express* **8**(5), 2732 (2017).
48. P. Zang, J. Wang, T. T. Hormel, L. Liu, D. Huang, and Y. Jia, "Automated segmentation of peripapillary retinal boundaries in OCT combining a convolutional neural network and a multi-weights graph search," *Biomed. Opt. Express* **10**(8), 4340 (2019).
49. J. Kugelman, D. Alonso-Caneiro, S. A. Read, S. J. Vincent, and M. J. Collins, "Automatic segmentation of OCT retinal boundaries using recurrent neural networks and graph search," *Biomed. Opt. Express* **9**(11), 5759 (2018).
50. J. Schottenhamml, E. M. Moult, S. B. Ploner, S. Chen, E. Novais, L. Husvogt, J. S. Duker, N. K. Waheed, J. G. Fujimoto, and A. K. Maier, "OCT-OCTA segmentation: combining structural and blood flow information to segment Bruch's membrane," *Biomed. Opt. Express* **12**(1), 84 (2021).
51. Y. Guo, T. T. Hormel, H. Xiong, J. Wang, T. S. Hwang, and Y. Jia, "Automated segmentation of retinal fluid volumes from structural and angiographic optical coherence tomography using deep learning," *Trans. Vis. Sci. Technol.* **9**(2), 54 (2020).
52. M. F. Kraus, B. Potsaid, M. A. Mayer, R. Bock, B. Baumann, J. J. Liu, J. Hornegger, and J. G. Fujimoto, "Motion correction in optical coherence tomography volumes on a per A-scan basis using orthogonal scan patterns," *Biomed. Opt. Express* **3**(6), 1182–1199 (2012).
53. A. Camino, M. Zhang, C. Dongye, A. D. Pechauer, T. S. Hwang, S. T. Bailey, B. Lujan, D. J. Wilson, D. Huang, and Y. Jia, "Automated registration and enhanced processing of clinical optical coherence tomography angiography," *Quant. Imaging Med. Surg.* **6**(4), 391–401 (2016).
54. P. Zang, G. Liu, M. Zhang, J. Wang, T. S. Hwang, D. J. Wilson, D. Huang, D. Li, and Y. Jia, "Automated three-dimensional registration and volume rebuilding for wide-field angiographic and structural optical coherence tomography," *J. Biomed. Opt.* **22**(2), 026001 (2017).
55. M. Heisler, S. Lee, Z. Mammo, Y. Jian, M. Ju, A. Merkur, E. Navajas, C. Balaratnasingam, M. F. Beg, and M. V. Sarunic, "Strip-based registration of serially acquired optical coherence tomography angiography," *J. Biomed. Opt.* **22**(3), 036007 (2017).
56. Y. Cheng, Z. Chu, and R. K. Wang, "Robust three-dimensional registration on optical coherence tomography angiography for speckle reduction and visualization," *Quant. Imaging Med. Surg.* **11**(3), 879–894 (2020).
57. A. F. Frangi, W. J. Niessen, K. L. Vincken, and M. A. Viergever, "Multiscale vessel enhancement filtering," in *Medical Image Computing and Computer-Assisted Intervention* (1998), Vol. 1496, pp. 130–137.
58. M. Chlebiej, I. Górczynska, A. Rutkowski, J. Kluczewski, T. Grzona, E. Pijewska, B. L. Sikorski, A. Szklumowska, and M. Szklumowski, "Quality improvement of OCT angiograms with elliptical directional filtering," *Biomed. Opt. Express* **10**(2), 1013 (2019).
59. J. Zhang, Y. Qiao, M. S. Sarabi, M. M. Khansari, J. K. Gahm, A. H. Kashani, and Y. Shi, "3D Shape Modeling and Analysis of Retinal Microvasculature in OCT-Angiography Images," *IEEE Trans. Med. Imaging* **39**(5), 1335–1346 (2020).
60. M. Gao, T. T. Hormel, J. Wang, Y. Guo, S. T. Bailey, T. S. Hwang, and Y. Jia, "An open-source deep learning network for reconstruction of high-resolution oct angiograms of retinal intermediate and deep capillary plexuses," *Trans. Vis. Sci. Technol.* **10**(13), 13–14 (2021).
61. M. Gao, Y. Guo, T. T. Hormel, J. Sun, T. S. Hwang, and Y. Jia, "Reconstruction of high-resolution 6×6-mm OCT angiograms using deep learning," *Biomed. Opt. Express* **11**(7), 3585 (2020).
62. M. Niederleithner, L. De Sisternes, H. Stino, A. Sedova, T. Schlegl, H. Bagherinia, A. Britten, P. Matten, U. Schmidt-Erfurth, A. Pollreisz, W. Drexler, R. A. Leitgeb, and T. Schmoll, "Ultra-widefield OCT angiography," *IEEE Trans. Med. Imaging* **42**(4), 1009–1020 (2023).
63. D. Matsunaga, J. Yi, C. A. Puliafito, and A. H. Kashani, "OCT angiography in healthy human subjects," *Ophthalmic Surg. Lasers Imaging Retin.* **45**(6), 510–515 (2014).
64. K. R. Mendis, C. Balaratnasingam, P. Yu, C. J. Barry, I. L. McAllister, S. J. Cringle, and D. yi Yu, "Correlation of histologic and clinical images to determine the diagnostic value of fluorescein angiography for studying retinal capillary detail," *Invest. Ophthalmol. Visual Sci.* **51**(11), 5864–5869 (2010).

65. R. F. Spaide and C. A. Curcio, "Evaluation of segmentation of the superficial and deep vascular layers of the retina by optical coherence tomography angiography instruments in normal eyes," *JAMA Ophthalmol.* **135**(3), 259–262 (2017).
66. R. F. Spaide, J. G. Fujimoto, N. K. Waheed, S. R. Sadda, and G. Staurenghi, "Optical coherence tomography angiography," *Prog. Retin. Eye Res.* **64**, 1–55 (2018).
67. S. C. Lee, S. Tran, A. Amin, L. S. Morse, A. Moshiri, S. S. Park, and G. Yiu, "Retinal vessel density in exudative and nonexudative age-related macular degeneration on optical coherence tomography angiography," *Am. J. Ophthalmol.* **212**, 7–16 (2020).
68. A. Y. Kim, Z. Chu, A. Shahidzadeh, R. K. Wang, C. A. Puliafito, and A. H. Kashani, "Quantifying microvascular density and morphology in diabetic retinopathy using spectral-domain optical coherence tomography angiography," *Invest. Ophthalmol. Visual Sci.* **57**(9), OCT362 (2016).
69. S. A. Agemy, N. K. Scripsma, C. M. Shah, T. Chui, P. M. Garcia, J. G. Lee, R. C. Gentile, Y. S. Hsiao, Q. Zhou, T. Ko, and R. B. Rosen, "Retinal vascular perfusion density mapping using optical coherence tomography angiography in normals and diabetic retinopathy patients," *Retina* **35**(11), 2353–2363 (2015).
70. T. Nishida, S. Moghimi, J. H. Wu, A. C. Chang, A. Diniz-Filho, A. Kamalipour, L. M. Zangwill, and R. N. Weinreb, "Association of initial optical coherence tomography angiography vessel density loss with faster visual field loss in glaucoma," *JAMA Ophthalmol.* **140**(4), 319–326 (2022).
71. A. Kamalipour, S. Moghimi, P. Khosravi, V. Mohammadmazdeh, T. Nishida, E. Micheletti, J. H. Wu, G. Mahmoudinezhad, E. H. F. Li, M. Christopher, L. Zangwill, T. Javidi, and R. N. Weinreb, "Combining optical coherence tomography and optical coherence tomography angiography longitudinal data for the detection of visual field progression in glaucoma," *Am. J. Ophthalmol.* **246**, 141–154 (2023).
72. H. L. Rao, Z. S. Pradhan, R. N. Weinreb, H. B. Reddy, M. Riyazuddin, S. Dasari, M. Palakurthy, N. K. Puttaiah, D. A. S. Rao, and C. A. B. Webers, "Regional comparisons of optical coherence tomography angiography vessel density in primary open-angle glaucoma," *Am. J. Ophthalmol.* **171**, 75–83 (2016).
73. Q. Zhang, K. A. Rezaei, S. S. Saraf, Z. Chu, F. Wang, and R. K. Wang, "Ultra-wide optical coherence tomography angiography in diabetic retinopathy," *Quant. Imaging Med. Surg.* **8**(8), 743–753 (2018).
74. M. B. Parodi, A. Rabiolo, M. V. Cincinelli, P. Iacono, F. Romano, and F. Bandello, "Quantitative analysis of optical coherence tomography angiography in adult-onset foveomacular vitelliform," *Retina* **38**(2), 237–244 (2018).
75. E. Wei, Y. Jia, O. Tan, B. Potsaid, J. J. Liu, W. J. Choi, J. G. Fujimoto, and D. Huang, "Parafoveal retinal vascular response to pattern visual stimulation assessed with OCT angiography," *PLoS One* **8**(12), e81343 (2013).
76. A. M. Hagag, J. I. E. Wang, K. Lu, G. Harman, R. G. Weleber, D. Huang, P. Yang, M. E. Pennesi, and Y. Jia, "Projection-resolved optical coherence tomographic angiography of retinal plexuses in retinitis pigmentosa," *Am. J. Ophthalmol.* **204**, 70–79 (2019).
77. S. S. Gao, Y. Jia, L. Liu, M. Zhang, H. L. Takusagawa, J. C. Morrison, and D. Huang, "Compensation for reflectance variation in vessel density quantification by optical coherence tomography angiography," *Invest. Ophthalmol. Visual Sci.* **57**(10), 4485–4492 (2016).
78. C. Bowd, A. Belghith, L. M. Zangwill, M. Christopher, M. H. Goldbaum, R. Fan, J. Rezapour, S. Moghimi, A. Kamalipour, H. Hou, and R. N. Weinreb, "Deep learning image analysis of optical coherence tomography angiography measured vessel density improves classification of healthy and glaucoma eyes," *Am. J. Ophthalmol.* **236**, 298–308 (2022).
79. Q. Wang, S. Chan, J. Y. Yang, B. You, Y. X. Wang, J. B. Jonas, and W. Bin Wei, "Vascular density in retina and choriocapillaris as measured by optical coherence tomography angiography," *Am. J. Ophthalmol.* **168**, 95–109 (2016).
80. Q. Zhang, J. B. Jonas, Q. Wang, S. Y. Chan, L. Xu, W. Bin Wei, and Y. X. Wang, "Optical coherence tomography angiography vessel density changes after acute intraocular pressure elevation," *Sci. Rep.* **8**(1), 6024 (2018).
81. P. Milani, G. Montesano, L. Rossetti, F. Bergamini, and A. Pece, "Vessel density, retinal thickness, and choriocapillaris vascular flow in myopic eyes on OCT angiography," *Graef's Arch. Clin. Exp. Ophthalmol.* **256**(8), 1419–1427 (2018).
82. A. Rabiolo, F. Gelormini, R. Sacconi, M. V. Cincinelli, G. Triolo, P. Bettin, K. Nouri-Mahdavi, F. Bandello, and G. Querques, "Comparison of methods to quantify macular and peripapillary vessel density in optical coherence tomography angiography," *PLoS One* **13**(10), e0205773 (2018).
83. J. Dong, Y. D. Jia, Q. Wu, S. Zhang, Y. Jia, D. Huang, and X. Wang, "Interchangeability and reliability of macular perfusion parameter measurements using optical coherence tomography angiography," *Br. J. Ophthalmol.* **101**(11), 1542–1549 (2017).
84. A. Rabiolo, F. Gelormini, A. Marchese, M. V. Cincinelli, G. Triolo, R. Sacconi, L. Querques, F. Bandello, and G. Querques, "Macular perfusion parameters in different angioblock sizes: Does the size matter in quantitative optical coherence tomography angiography?" *Invest. Ophthalmol. Visual Sci.* **59**(1), 231–237 (2018).
85. F. Corvi, M. Pellegrini, S. Erba, M. Cozzi, G. Staurenghi, and A. Giani, "Reproducibility of vessel density, fractal dimension, and foveal avascular zone using 7 different optical coherence tomography angiography devices," *Am. J. Ophthalmol.* **186**, 25–31 (2018).
86. M. Al-sheikh, T. C. Tepelus, T. Nazikyan, and S. R. V. R. Sadda, "Repeatability of automated vessel density measurements using optical coherence tomography angiography," *Br. J. Ophthalmol.* **101**(4), 449–452 (2017).

87. Q. You, W. R. Freeman, R. N. Weinreb, L. Zangwill, P. I. C. Manalastas, L. J. Saunders, and E. Nudleman, "Reproducibility of vessel density measurement with optical coherence tomography angiography in eyes with and without retinopathy," *Retina* **37**(8), 1475–1482 (2017).
88. Y. Ma, H. Hao, J. Xie, H. Fu, J. Zhang, J. Yang, Z. Wang, J. Liu, Y. Zheng, and Y. Zhao, "ROSE: a retinal OCT-angiography vessel segmentation dataset and new model," *IEEE Trans. Med. Imaging* **40**(3), 928–939 (2021).
89. B. Wang, A. Camino, S. Pi, Y. Guo, J. Wang, D. Huang, T. S. Hwang, and Y. Jia, "Three-dimensional structural and angiographic evaluation of foveal ischemia in diabetic retinopathy: method and validation," *Biomed. Opt. Express* **10**(7), 3522–3532 (2019).
90. S. Chen, E. M. Moult, L. M. Zangwill, R. N. Weinreb, and J. G. Fujimoto, "Geometric perfusion deficits: a novel OCT angiography biomarker for diabetic retinopathy based on oxygen diffusion," *Am. J. Ophthalmol.* **222**, 256–270 (2021).
91. M. Zhang, T. S. Hwang, C. Dongye, D. J. Wilson, D. Huang, and Y. Jia, "Automated quantification of nonperfusion in three retinal plexuses using projection-resolved optical coherence tomography angiography in diabetic retinopathy," *Invest. Ophthalmol. Visual Sci.* **57**(13), 5101–5106 (2016).
92. J. Wang, T. T. Hormel, Q. You, Y. Guo, X. Wang, L. Chen, T. S. Hwang, and Y. Jia, "Robust non-perfusion area detection in three retinal plexuses using convolutional neural network in OCT angiography," *Biomed. Opt. Express* **11**(1), 330–345 (2020).
93. M. Heisler, F. Chan, Z. Mammo, C. Balaratnasingam, P. Prentasic, G. Docherty, M. Ju, S. Rajapakse, S. Lee, A. Merkur, A. Kirker, D. Albiani, D. Maberley, K. B. Freund, M. F. Beg, S. Loncaric, M. V. Sarunic, and E. V. Navajas, "Deep learning vessel segmentation and quantification of the foveal avascular zone using commercial and prototype OCT-A platforms," *arXiv*, arXiv:1909.11289 (2019).
94. Y. Guo, A. Camino, J. Wang, D. Huang, T. S. Hwang, and Y. Jia, "MEDnet, a neural network for automated detection of avascular area in OCT angiography," *Biomed. Opt. Express* **9**(11), 5147–5158 (2018).
95. Y. Guo, T. T. Hormel, H. Xiong, B. Wang, A. Camino, J. Wang, D. Huang, T. S. Hwang, and Y. Jia, "Development and validation of a deep learning algorithm for distinguishing the nonperfusion area from signal reduction artifacts on OCT angiography," *Biomed. Opt. Express* **10**(7), 3257 (2019).
96. T. S. Hwang, A. M. Hagag, J. Wang, M. Zhang, A. Smith, D. J. Wilson, D. Huang, and Y. Jia, "Automated quantification of nonperfusion areas in 3 vascular plexuses with optical coherence tomography angiography in eyes of patients with diabetes," *JAMA Ophthalmol.* **136**(8), 929–936 (2018).
97. T. S. Hwang, Z. Miao, K. Bhavsar, Z. Xinbo, J. P. Campbell, P. Lin, S. T. Bailey, C. J. Flaxel, A. K. Lauer, D. J. Wilson, D. Huang, and Y. Jia, "Visualization of 3 distinct retinal plexuses by projection-resolved optical coherence tomography angiography in diabetic retinopathy," *JAMA Ophthalmol.* **134**(12), 1411–1419 (2016).
98. N. L. Decker, B. V. Duffy, G. O. Boughanem, H. Fukuyama, D. Castellanos Canales, P. L. Nesper, M. K. Gill, and A. A. Fawzi, "Macular perfusion deficits on OCTA correlate with non-perfusion on ultrawide-field FA in diabetic retinopathy," *Ophthalmol. Retin.* **7**, 692–702 (2023).
99. P. L. Nesper, P. K. Roberts, A. C. Onishi, H. Chai, L. Liu, L. M. Jampol, and A. A. Fawzi, "Quantifying microvascular abnormalities with increasing severity of diabetic retinopathy using optical coherence tomography angiography," *Invest. Ophthalmol. Visual Sci.* **58**(6), BIO307 (2017).
100. C. W. Spraul, G. E. Lang, G. K. Lang, and H. E. Grossniklaus, "Morphometric changes of the choriocapillaris and the choroidal vasculature in eyes with advanced glaucomatous changes," *Vision Res.* **42**(7), 923–932 (2002).
101. C. A. Moreira-Neto, E. M. Moult, J. G. Fujimoto, N. K. Waheed, and D. Ferrara, "Choriocapillaris loss in advanced age-related macular degeneration," *J. Ophthalmol.* **2018**, 1–6 (2018).
102. R. Lejoyeux, J. Benillouche, J. Ong, M. H. Errera, E. A. Rossi, S. R. Singh, K. K. Dansingani, S. da Silva, D. Sinha, J. A. Sahel, K. B. Freund, S. V. R. Sadda, G. A. Lutty, and J. Chhablani, "Choriocapillaris: Fundamentals and advancements," *Prog. Retin. Eye Res.* **87**, 100997 (2022).
103. M. A. Klufas, N. Phasukkijwatana, N. A. Iafe, P. S. Prasad, A. Agarwal, V. Gupta, W. Ansari, F. Pichi, S. Srivastava, K. B. Freund, S. V. R. Sadda, and D. Sarraf, "Optical Coherence Tomography Angiography Reveals Choriocapillaris Flow Reduction in Placoid Chorioretinitis," *Ophthalmol. Retin.* **1**(1), 77–91 (2017).
104. Z. Chu, Q. Zhang, G. Gregori, P. J. Rosenfeld, and R. K. Wang, "Guidelines for imaging the choriocapillaris using OCT angiography," *Am. J. Ophthalmol.* **222**, 92–101 (2021).
105. I. Byon, M. Nassisi, E. Borrelli, and S. R. Sadda, "Impact of slab selection on quantification of choriocapillaris flow deficits by optical coherence tomography angiography," *Am. J. Ophthalmol.* **208**, 397–405 (2019).
106. W. J. Choi, K. J. Mohler, B. Potsaid, C. D. Lu, J. J. Liu, V. Jayaraman, A. E. Cable, J. S. Duker, R. Huber, and J. G. Fujimoto, "Choriocapillaris and choroidal microvasculature imaging with ultrahigh speed OCT angiography," *PLoS One* **8**(12), e81499 (2013).
107. J. Scharf, G. Corradetti, F. Corvi, S. Sadda, and D. Sarraf, "Optical coherence tomography angiography of the choriocapillaris in age-related macular degeneration," *J. Clin. Med.* **10**(4), 751 (2021).
108. F. Corvi, L. Su, and S. R. Sadda, "Evaluation of the inner choroid using OCT angiography," *Eye* **35**(1), 110–120 (2021).
109. G. Ledesma-Gil, P. Fernández-Avellaneda, and R. F. Spaide, "Swept-source optical coherence tomography angiography imaging of the choriocapillaris," *Retina* **41**(7), 1373–1378 (2021).

110. Q. Zhang, F. Zheng, E. H. Motulsky, G. Gregori, Z. Chu, C. L. Chen, C. Li, L. De Sisternes, M. Durbin, P. J. Rosenfeld, and R. K. Wang, "A novel strategy for quantifying choriocapillaris flow voids using swept-source OCT angiography," *Invest. Ophthalmol. Visual Sci.* **59**(1), 203–211 (2018).
111. Z. Chu, G. Gregori, P. J. Rosenfeld, and R. K. Wang, "Quantification of choriocapillaris with optical coherence tomography angiography: a comparison study," *Am. J. Ophthalmol.* **208**, 111–123 (2019).
112. A. R. Alagorie, A. Verma, M. Nassisi, and S. R. Sadda, "Quantitative assessment of choriocapillaris flow deficits in eyes with advanced age-related macular degeneration versus healthy eyes," *Am. J. Ophthalmol.* **205**, 132–139 (2019).
113. F. Zheng, Q. Zhang, Y. Shi, J. F. Russell, E. H. Motulsky, J. T. Banta, Z. Chu, H. Zhou, N. A. Patel, L. de Sisternes, M. K. Durbin, W. Feuer, G. Gregori, R. Wang, and P. J. Rosenfeld, "age-dependent changes in the macular choriocapillaris of normal eyes imaged with swept-source optical coherence tomography angiography," *Am. J. Ophthalmol.* **200**, 110–122 (2019).
114. R. F. Spaide, "Choriocapillaris signal voids in maternally inherited diabetes and deafness and in pseudoxanthoma elasticum," *Retina* **37**(11), 2008–2014 (2017).
115. N. Phansalkar, S. More, A. Sabale, and M. Joshi, "Adaptive local thresholding for detection of nuclei in diversity stained cytology images," *ICCS 2011 - 2011 Int. Conf. Commun. Signal Process.* 218–220 (2011).
116. Z. Chu, Y. Cheng, Q. Zhang, H. Zhou, Y. Dai, Y. Shi, G. Gregori, P. J. Rosenfeld, and R. K. Wang, "Quantification of choriocapillaris with phansalkar local thresholding: pitfalls to avoid," *Am. J. Ophthalmol.* **213**, 161–176 (2020).
117. E. M. Moult, Y. Shi, Q. Zhang, L. Wang, R. Mazumder, S. Chen, Z. Chu, W. Feuer, N. K. Waheed, G. Gregori, R. K. Wang, P. J. Rosenfeld, and J. G. Fujimoto, "Analysis of correlations between local geographic atrophy growth rates and local OCT angiography-measured choriocapillaris flow deficits," *Biomed. Opt. Express* **12**(7), 4573 (2021).
118. K. Nattagh, H. Zhou, N. Rinella, Q. Zhang, Y. Dai, K. G. Foote, C. Keiner, M. Deiner, J. L. Duncan, T. C. Porco, R. K. Wang, and D. M. Schwartz, "Oct angiography to predict geographic atrophy progression using choriocapillaris flow void as a biomarker," *Trans. Vis. Sci. Technol.* **9**(7), 6 (2020).
119. Q. Zhang, Y. Shi, H. Zhou, G. Gregori, Z. Chu, F. Zheng, E. H. Motulsky, L. de Sisternes, M. Durbin, P. J. Rosenfeld, and R. K. Wang, "Accurate estimation of choriocapillaris flow deficits beyond normal intercapillary spacing with swept source OCT angiography," *Quant. Imaging Med. Surg.* **8**(7), 658–666 (2018).
120. G. Ledesma-Gil, P. Fernández-Avellaneda, and R. F. Spaide, "Swept-source optical coherence tomography angiography image compensation of the choriocapillaris induces artifacts," *Retina* **40**(10), 1865–1872 (2020).
121. P. L. Nesper and A. A. Fawzi, "New method for reducing artifactual flow deficits caused by compensation techniques in the choriocapillaris with optical coherence tomography angiography," *Retina* **42**(2), 328–335 (2022).
122. R. F. Spaide, "Choriocapillaris flow features follow a power law distribution: implications for characterization and mechanisms of disease progression," *Am. J. Ophthalmol.* **170**, 58–67 (2016).
123. F. Corvi, G. Corradetti, L. Tiosano, J. A. McLaughlin, T. K. Lee, and S. R. Sadda, "Topography of choriocapillaris flow deficit predicts development of neovascularization or atrophy in age-related macular degeneration," *Graef's Arch. Clin. Exp. Ophthalmol.* **259**(10), 2887–2895 (2021).
124. I. Byon, Y. Ji, A. R. Alagorie, L. Tiosano, and S. R. Sadda, "Topographic assessment of choriocapillaris flow deficits in the intermediate age-related macular degeneration eyes with hyporeflective cores inside drusen," *Retina* **41**(2), 393–401 (2021).
125. A. R. Alagorie, A. Verma, M. Nassisi, M. Nittala, S. Velaga, L. Tiosano, and S. R. Sadda, "Quantitative assessment of choriocapillaris flow deficits surrounding choroidal neovascular membranes," *Retina* **40**(11), 2106–2112 (2020).
126. Y. Shi, Q. Zhang, H. Zhou, L. Wang, Z. Chu, X. Jiang, M. Shen, M. Thulliez, C. Lyu, W. Feuer, L. de Sisternes, M. K. Durbin, G. Gregori, R. K. Wang, and P. J. Rosenfeld, "Correlations between choriocapillaris and choroidal measurements and the growth of geographic atrophy using swept source oct imaging," *Am. J. Ophthalmol.* **224**, 321–331 (2021).
127. G. H. Bresnick, R. Condit, S. Syrjala, M. Palta, A. Groo, and K. Korth, "Abnormalities of the foveal avascular zone in diabetic retinopathy," *Arch. Ophthalmol.* **102**(9), 1286–1293 (1984).
128. M. B. Parodi, F. Visintin, P. Della Rupe, and G. Ravalico, "Foveal avascular zone in macular branch retinal vein occlusion," *Int. Ophthalmol.* **19**(1), 25–28 (1995).
129. R. J. Sanders, G. C. Brown, R. B. Rosenstein, and L. Magargal, "Foveal avascular zone diameter and sickle cell disease," *Arch. Ophthalmol.* **109**(6), 812–815 (1991).
130. B. D. Krawitz, S. Mo, L. S. Geyman, S. A. Agemy, N. K. Scripssema, P. M. Garcia, T. Y. P. Chui, and R. B. Rosen, "Acircularity index and axis ratio of the foveal avascular zone in diabetic eyes and healthy controls measured by optical coherence tomography angiography," *Vision Res.* **139**, 177–186 (2017).
131. T. E. De Carlo, A. T. Chin, M. A. Bonini Filho, M. Adhi, L. Branchini, D. A. Salz, C. R. Baumal, C. Crawford, E. Reichel, A. J. Witkin, J. S. Duker, and N. K. Waheed, "Detection of microvascular changes in eyes of patients with diabetes but not clinical diabetic retinopathy using optical coherence tomography angiography," *Retina* **35**(11), 2364–2370 (2015).
132. F. J. Freiberg, M. Pfau, J. Wons, M. A. Wirth, M. D. Becker, and S. Michels, "Optical coherence tomography angiography of the foveal avascular zone in diabetic retinopathy," *Graef's Arch. Clin. Exp. Ophthalmol.* **254**(6), 1051–1058 (2016).

133. H. Shiihara, H. Terasaki, S. Sonoda, N. Kakiuchi, Y. Shinohara, M. Tomita, and T. Sakamoto, "Objective evaluation of size and shape of superficial foveal avascular zone in normal subjects by optical coherence tomography angiography," *Sci. Rep.* **8**(1), 10143 (2018).
134. P. Carpineto, R. Mastropasqua, G. Marchini, L. Toto, M. Di Nicola, and L. Di Antonio, "Reproducibility and repeatability of foveal avascular zone measurements in healthy subjects by optical coherence tomography angiography," *Br. J. Ophthalmol.* **100**(5), 671–676 (2016).
135. C. La Spina, A. Carnevali, A. Marchese, G. Querques, and F. Bandello, "Reproducibility and reliability of optical coherence tomography angiography for foveal avascular zone evaluation and measurement in different settings," *Retina* **37**(9), 1636–1641 (2017).
136. R. Linderman, A. E. Salmon, M. Strampe, M. Russillo, J. Khan, and J. Carroll, "Assessing the accuracy of foveal avascular zone measurements using optical coherence tomography angiography: Segmentation and scaling," *Trans. Vis. Sci. Technol.* **6**(3), 16 (2017).
137. G. N. Magrath, E. A. T. Say, K. Sioufi, S. Ferenczy, W. A. Samara, and C. L. Shields, "Variability in foveal avascular zone and capillary density using optical coherence tomography angiography machines in healthy eyes," *Retina* **37**(11), 2102–2111 (2017).
138. R. Mirshahi, P. Anvari, H. Riazi-Esfahani, M. Sardarinia, M. Naseripour, and K. G. Falavarjani, "Foveal avascular zone segmentation in optical coherence tomography angiography images using a deep learning approach," *Sci. Rep.* **11**(1), 1031–1038 (2021).
139. D. Yang, Z. Tang, A. Ran, T. X. Nguyen, S. Szeto, J. Chan, C. Y. K. Wong, V. Hui, K. Tsang, C. K. M. Chan, C. C. Tham, S. Sivaprasad, T. Y. Y. Lai, and C. Y. Cheung, "Assessment of parafoveal diabetic macular ischemia on optical coherence tomography angiography images to predict diabetic retinal disease progression and visual acuity deterioration," *JAMA Ophthalmol.* **141**, 641–649 (2023).
140. L. Kuehlewein, T. C. Tepelus, L. An, M. K. Durbin, S. Srinivas, and S. R. Sadda, "Noninvasive visualization and analysis of the human parafoveal capillary network using swept source OCT optical microangiography," *Invest. Ophthalmol. Visual Sci.* **56**(6), 3984–3988 (2015).
141. T. Y. P. Chui, D. A. VanNasdale, A. E. Elsner, and S. A. Burns, "The association between the foveal avascular zone and retinal thickness," *Invest. Ophthalmol. Visual Sci.* **55**(10), 6870–6877 (2014).
142. R. Flores, A. Carneiro, M. Vieira, S. Tenreiro, and M. C. Seabra, "Age-related macular degeneration: pathophysiology, management, and future perspectives," *Ophthalmologica* **244**(6), 495–511 (2021).
143. R. F. Spaide, K. Ohno-Matsui, and L. A. Yannuzzi, *Pathologic Myopia* (Springer, 2014).
144. M. A. Bonini Filho, T. E. De Carlo, D. Ferrara, M. Adhi, C. R. Baumal, A. J. Witkin, E. Reichel, J. S. Duker, and N. K. Waheed, "Association of choroidal neovascularization and central serous chorioretinopathy with optical coherence tomography angiography," *JAMA Ophthalmol.* **133**(8), 899–906 (2015).
145. M. Srour, G. Querques, and E. H. Souied, "Optical coherence tomography angiography of idiopathic polypoidal choroidal vasculopathy," *Dev. Ophthalmol.* **56**, 71–76 (2016).
146. S. Mehta, "Age-related macular degeneration," *Lancet* **392**(10153), 1147–1159 (2018).
147. P. J. Rosenfeld, D. M. Brown, J. S. Heier, D. S. Boyer, P. K. Kaiser, C. Y. CHung, and R. Y. Kim, "Ranibizumab for neovascular age-related macular degeneration," *N. Engl. J. Med.* **355**(14), 1419–1431 (2006).
148. J. M. Kim, H. J. Cho, Y. Kim, S. H. Jung, D. W. Lee, and J. W. Kim, "Responses of types 1 and 2 neovascularization in age-related macular degeneration to anti-vascular endothelial growth factor treatment: optical coherence tomography angiography analysis," *Semin. Ophthalmol.* **34**(3), 168–176 (2019).
149. R. Patel, J. Wang, J. P. Campbell, L. Kiang, A. Lauer, C. Flaxel, T. Hwang, B. Lujan, D. Huang, S. T. Bailey, and Y. Jia, "Classification of choroidal neovascularization using projection-resolved optical coherence tomographic angiography," *Invest. Ophthalmol. Visual Sci.* **59**(10), 4285–4291 (2018).
150. P. L. Nesper, B. T. Soetikno, A. D. Treister, and A. A. Fawzi, "Volume-rendered projection-resolved OCT angiography: 3D lesion complexity is associated with therapy response in wet age-related macular degeneration," *Invest. Ophthalmol. Visual Sci.* **59**(5), 1944–1952 (2018).
151. D. Huang, Y. Jia, M. Rispoli, O. Tan, and B. Lumbroso, "Optical coherence tomography angiography of time course of choroidal neovascularization in response to anti-angiogenic treatment," *Retina* **35**(11), 2260–2264 (2015).
152. R. F. Spaide, "Optical coherence tomography angiography signs of vascular abnormalization with antiangiogenic therapy for choroidal neovascularization," *Am. J. Ophthalmol.* **160**(1), 6–16 (2015).
153. N. W. Muakkassa, A. T. Chin, T. De Carlo, K. A. Klein, C. R. Baumal, A. J. Witkin, J. S. Duker, and N. K. Waheed, "Characterizing the effect of anti-vascular endothelial growth factor therapy on treatment-naïve choroidal neovascularization using optical coherence tomography angiography," *Retina* **35**(11), 2252–2259 (2015).
154. N. V. Palejwala, Y. Jia, S. S. Gao, L. Liu, C. J. Flaxel, T. S. Hwang, A. K. Lauer, D. J. Wilson, D. Huang, and S. T. Bailey, "Detection of nonexudative choroidal neovascularization in age-related macular degeneration with optical coherence tomography angiography," *Retina* **35**(11), 2204–2211 (2015).
155. S. T. Bailey, O. Thaware, J. Wang, A. M. Hagag, X. Zhang, C. J. Flaxel, A. K. Lauer, T. S. Hwang, P. Lin, D. Huang, and Y. Jia, "Detection of nonexudative choroidal neovascularization and progression to exudative choroidal neovascularization using OCT angiography," *Ophthalmol. Retin.* **3**(8), 629–636 (2019).
156. J. Wang, T. T. Hormel, K. Tsuboi, X. Wang, X. Ding, X. Peng, D. Huang, S. T. Bailey, and Y. Jia, "Deep learning for diagnosing and segmenting choroidal neovascularization in OCT angiography in a large real-world data set," *Trans. Vis. Sci. Technol.* **12**(4), 15 (2023).

157. J. Wang, T. T. Hormel, L. Gao, P. Zang, Y. Guo, X. Wang, S. T. Bailey, and Y. Jia, "Automated diagnosis and segmentation of choroidal neovascularization in OCT angiography using deep learning," *Biomed. Opt. Express* **11**(2), 927 (2020).
158. J. F. Russell, H. W. Flynn, J. Sridhar, J. H. Townsend, Y. Shi, K. C. Fan, N. L. Scott, J. W. Hinkle, C. Lyu, G. Gregori, S. R. Russell, and P. J. Rosenfeld, "Distribution of diabetic neovascularization on ultra-widefield fluorescein angiography and on simulated widefield OCT angiography," *Am. J. Ophthalmol.* **207**, 110–120 (2019).
159. A. W. Stitt, T. M. Curtis, M. Chen, R. J. Medina, G. J. McKay, A. Jenkins, T. A. Gardiner, T. J. Lyons, H. P. Hammes, R. Simó, and N. Lois, "The progress in understanding and treatment of diabetic retinopathy," *Prog. Retin. Eye Res.* **51**, 156–186 (2016).
160. S. Ni, X. Wei, R. Ng, S. Ostmo, M. F. Chiang, D. Huang, Y. Jia, J. P. Campbell, and Y. Jian, "High-speed and widefield handheld swept-source OCT angiography with a VCSEL light source," *Biomed. Opt. Express* **12**(6), 3553 (2021).
161. J. G. Gross, A. R. Glassman, D. Liu, J. K. Sun, A. N. Antoszyk, C. W. Baker, N. M. Bressler, M. J. Elman, F. L. Ferris, T. W. Gardner, L. M. Jampol, D. F. Martin, M. Melia, C. R. Stockdale, and R. W. Beck, "Five-year outcomes of panretinal photocoagulation vs intravitreous ranibizumab for proliferative diabetic retinopathy: a randomized clinical trial," *JAMA Ophthalmol.* **136**(10), 1138–1148 (2018).
162. K. Tsuboi, M. Mazloumi, Y. Guo, J. Wang, C. J. Flaxel, S. T. Bailey, D. Huang, Y. Jia, and T. S. Hwang, "Utility of en face OCT for the detection of clinically unsuspected retinal neovascularization in patients with diabetic retinopathy," *Ophthalmol. Retin.* **141**683–691 (2023).
163. T. S. Hwang, Y. Jia, S. S. Gao, S. T. Bailey, A. K. Lauer, C. J. Flaxel, D. J. Wilson, and D. Huang, "Optical coherence tomography angiography features in diabetic retinopathy," *Retina* **35**(11), 2371–2376 (2015).
164. F. He and W. Yu, "Longitudinal neovascular changes on optical coherence tomography angiography in proliferative diabetic retinopathy treated with panretinal photocoagulation alone versus with intravitreal conbercept plus panretinal photocoagulation: a pilot study," *Eye* **34**(8), 1413–1418 (2020).
165. M. Arya, O. Sorour, J. Chaudhri, Y. Alibhai, N. K. Waheed, J. S. Duker, and C. R. Baumal, "Distinguishing intraretinal microvascular abnormalities from retinal neovascularization using optical coherence tomography angiography," *Retina* **40**(9), 1686–1695 (2020).
166. P. Henkind and G. N. Wise, "Retinal neovascularization, collaterals, and vascular shunts," *Br. J. Ophthalmol.* **58**(4), 413–422 (1974).
167. A. H. Kashani, S. Y. Lee, A. Moshfeghi, M. K. Durbin, and C. A. Puliafito, "Optical coherence tomography angiography of retinal venous occlusion," *Retina* **35**(11), 2323–2331 (2015).
168. K. Tsuboi, H. Sasajima, and M. Kamei, "Collateral vessels in branch retinal vein occlusion: anatomic and functional analyses by optical coherence tomography angiography," *Ophthalmol. Retin.* **37**67–776 (2019).
169. N. Suzuki, Y. Hirano, M. Yoshida, T. Tomiyasu, A. Uemura, T. Yasukawa, and Y. Ogura, "Microvascular abnormalities on optical coherence tomography angiography in macular edema associated with branch retinal vein occlusion," *Am. J. Ophthalmol.* **161**, 126–132.e1 (2016).
170. K. B. Freund, D. Sarraf, B. C. S. Leong, S. T. Garrity, K. K. Vupparaboina, and K. K. Dansingani, "Association of optical coherence tomography angiography of collaterals in retinal vein occlusion with major venous outflow through the deep vascular complex," *JAMA Ophthalmol.* **136**(11), 1262–1270 (2018).
171. Early Treatment of Diabetic Retinopathy Research Group, "Grading diabetic retinopathy from stereoscopic color fundus photographs—an extension of the modified airlie house classification: ETDRS report number 10," *Ophthalmology* **98**(5), 786–806 (1991).
172. K. B. Schaal, M. R. Munk, I. Wyssmueller, L. E. Berger, M. S. Zinkernagel, and S. Wolf, "Vascular abnormalities in diabetic retinopathy assessed with swept-source optical coherence tomography angiography widefield imaging," *Retina* **39**(1), 79–87 (2019).
173. O. A. Sorour, N. Mehta, C. R. Baumal, A. Ishibazawa, K. Liu, E. K. Konstantinou, S. Martin, P. Braun, A. Y. Alibhai, M. Arya, A. J. Witkin, J. S. Duker, and N. K. Waheed, "Morphological changes in intraretinal microvascular abnormalities after anti-VEGF therapy visualized on optical coherence tomography angiography," *Eye Vis.* **7**(1), 29 (2020).
174. J. Moore, S. Bagley, G. Ireland, D. McLeod, and M. E. Boulton, "Three dimensional analysis of microaneurysms in the human diabetic retina," *J. Anat.* **194**(1), 89–100 (1999).
175. A. W. Stitt, T. A. Gardiner, and D. B. Archer, "Histological and ultrastructural investigation of retinal microaneurysm development in diabetic patients," *Br. J. Ophthalmol.* **79**(4), 362–367 (1995).
176. D. A. Antonetti, R. Klein, and T. W. Gardner, "Diabetic retinopathy," *N. Engl. J. Med.* **366**(13), 1227–1239 (2012).
177. D. R. Matsunaga, J. J. Yi, L. O. De Koo, H. Ameri, C. A. Puliafito, and A. H. Kashani, "Optical coherence tomography angiography of diabetic retinopathy in human subjects," *Ophthalmic Surg. Lasers Imaging Retin.* **46**(8), 796–805 (2015).
178. S. Parrulli, F. Corvi, M. Cozzi, D. Monteduro, F. Zicarelli, and G. Staurenghi, "Microaneurysms visualisation using five different optical coherence tomography angiography devices compared to fluorescein angiography," *Br. J. Ophthalmol.* **105**(4), 526–530 (2021).
179. Y. Kaizu, S. Nakao, I. Wada, M. Arima, M. Yamaguchi, K. Ishikawa, M. Akiyama, J. Kishimoto, T. Hisatomi, and K. H. Sonoda, "Microaneurysm imaging using multiple en face oct angiography image averaging: morphology and visualization," *Ophthalmol. Retin.* **4**(2), 175–186 (2020).

180. M. Stattin, A. M. Haas, D. Ahmed, U. Stolba, A. Graf, K. Krepler, and S. Ansari-Shahrezaei, "Detection rate of diabetic macular microaneurysms comparing dye-based angiography and optical coherence tomography angiography," *Sci. Rep.* **10**(1), 16274–16278 (2020).
181. D. A. Salz, T. E. De Carlo, M. Adhi, E. Moult, W. Choi, C. R. Baumal, A. J. Witkin, J. S. Duker, J. G. Fujimoto, and N. K. Waheed, "Select features of diabetic retinopathy on swept-source optical coherence tomographic angiography compared with fluorescein angiography and normal eyes," *JAMA Ophthalmol.* **134**(6), 644–650 (2016).
182. M. Gao, T. T. Hormel, Y. Guo, K. Tsuboi, C. J. Flaxel, D. Huang, T. S. Hwang, and Y. Jia, "Active and inactive microaneurysms identified and characterized by structural and angiographic optical coherence tomography," *arXiv*, arXiv:2303.13611 (2023).
183. V. Schreur, A. Domanian, B. Liefers, F. G. Venhuizen, B. J. Klevering, C. B. Hoyng, E. K. De Jong, and T. Theelen, "Morphological and topographical appearance of microaneurysms on optical coherence tomography angiography," *Br. J. Ophthalmol.* **103**(5), 630–635 (2019).
184. M. Parravano, D. De Geronimo, F. Scarinci, L. Querques, G. Virgili, J. M. Simonett, M. Varano, F. Bandello, and G. Querques, "Diabetic microaneurysms internal reflectivity on spectral-domain optical coherence tomography and optical coherence tomography angiography detection," *Am. J. Ophthalmol.* **179**, 90–96 (2017).
185. M. Parravano, D. De Geronimo, F. Scarinci, G. Virgili, L. Querques, M. Varano, F. Bandello, and G. Querques, "Progression of diabetic microaneurysms according to the internal reflectivity on structural optical coherence tomography and visibility on optical coherence tomography angiography," *Am. J. Ophthalmol.* **198**, 8–16 (2019).
186. J. Lee and R. Rosen, "Optical coherence tomography angiography in diabetes," *Curr. Diab. Rep.* **16**(12), 123 (2016).
187. A. Ishibazawa, T. Nagaoka, A. Takahashi, T. Omae, T. Tani, K. Sogawa, H. Yokota, and A. Yoshida, "Optical coherence tomography angiography in diabetic retinopathy: A prospective pilot study," *Am. J. Ophthalmol.* **160**(1), 35–44.e1 (2015).
188. Y. Guo, T. T. Hormel, L. Gao, Q. You, B. Wang, C. J. Flaxel, S. T. Bailey, D. Choi, D. Huang, T. S. Hwang, and Y. Jia, "Quantification of Nonperfusion Area in Montaged Widefield OCT Angiography Using Deep Learning in Diabetic Retinopathy," *Ophthalmol. Sci.* **1**(2), 100027 (2021).
189. L. R. De Pretto, E. M. Moult, A. Y. Alibhai, O. M. Carrasco-Zevallos, S. Chen, B. K. Lee, A. J. Witkin, C. R. Baumal, E. Reichel, A. Z. de Freitas, J. S. Duker, N. K. Waheed, and J. G. Fujimoto, "Controlling for artifacts in widefield optical coherence tomography angiography measurements of non-perfusion area," *Sci. Rep.* **9**(1), 9096 (2019).
190. X. Wei, T. T. Hormel, Y. Guo, and Y. Jia, "75-degree non-mydriatic single-volume optical coherence tomographic angiography," *Biomed. Opt. Express* **10**(12), 6286–6295 (2019).
191. M. Gao, Y. Guo, T. T. Hormel, K. Tsuboi, G. Pacheco, D. Poole, S. T. Bailey, C. J. Flaxel, D. Huang, T. S. Hwang, and Y. Jia, "A deep learning network for classifying arteries and veins in montaged widefield OCT angiograms," *Ophthalmol. Sci.* **2**(2), 100149 (2022).
192. M. Alam, D. Le, T. Son, J. I. Lim, and X. Yao, "AV-Net: deep learning for fully automated artery-vein classification in optical coherence tomography angiography," *Biomed. Opt. Express* **11**(9), 5249 (2020).
193. A. Pinhas, J. V. Migacz, D. B. Zhou, M. V. Castanos Toral, O. Otero-Marquez, S. Israel, V. Sun, P. N. Gillette, N. Sredar, A. Dubra, J. Glassberg, R. B. Rosen, and T. Y. P. Chui, "Insights into Sickle Cell Disease through the Retinal Microvasculature," *Ophthalmol. Sci.* **2**(4), 100196 (2022).
194. A. Yarmohammadi, L. M. Zangwill, A. Diniz-Filho, M. H. Suh, S. Yousefi, L. J. Saunders, A. Belghith, P. I. C. Manalastas, F. A. Medeiros, and R. N. Weinreb, "Relationship between optical coherence tomography angiography vessel density and severity of visual field loss in glaucoma," *Ophthalmology* **123**(12), 2498–2508 (2016).
195. E. J. Lee, T. W. Kim, J. A. Kim, and J. A. Kim, "Central visual field damage and parapapillary choroidal microvasculature dropout in primary open-angle glaucoma," *Ophthalmology* **125**(4), 588–596 (2018).
196. A. Roorda, "Optoretinography is coming of age," *Proc. Natl. Acad. Sci. U. S. A.* **118**(51), 14–16 (2021).
197. G. Ma, T. Son, T. H. Kim, and X. Yao, "In vivo optoretinography of phototransduction activation and energy metabolism in retinal photoreceptors," *J. Biophotonics* **14**(5), 1–8 (2021).
198. A. Lassoud, F. Zhang, K. Kurokawa, Y. Liu, M. T. Bernucci, J. A. Crowell, and D. T. Miller, "Cone photoreceptor dysfunction in retinitis pigmentosa revealed by optoretinography," *Proc. Natl. Acad. Sci. U. S. A.* **118**(47), 1–12 (2021).
199. D. Le, M. Alam, C. Yao, J. I. Lim, R. V. P. Chan, D. Toslak, and X. Yao, "Transfer learning for automated OCTA detection of diabetic retinopathy," *Transl. Vis. Sci. Technol.* **9**, 35 (2019).
200. M. Heisler, S. Karst, J. Lo, Z. Mammo, T. Yu, S. Warner, D. Maberley, M. F. Beg, E. V. Navajas, and M. V. Sarunic, "Ensemble deep learning for diabetic retinopathy detection using optical coherence tomography angiography," *Trans. Vis. Sci. Technol.* **9**(2), 20 (2020).
201. P. Zang, L. Gao, T. T. Hormel, J. Wang, Q. You, T. S. Hwang, and Y. Jia, "DCardnet: diabetic retinopathy classification at multiple depths based on structural and angiographic optical coherence tomography," *IEEE Transactions on Biomedical Engineering* **68**, 1859 (2020).
202. J. Lo, T. T. Yu, D. Ma, P. Zang, J. P. Owen, Q. Zhang, R. K. Wang, M. F. Beg, A. Y. Lee, Y. Jia, and M. V. Sarunic, "Federated learning for microvasculature segmentation and diabetic retinopathy classification of OCT data," *Ophthalmol. Sci.* **1**(4), 100069 (2021).
203. P. Zang, T. T. Hormel, X. Wang, K. Tsuboi, D. Huang, T. S. Hwang, and Y. Jia, "A diabetic retinopathy classification framework based on deep-learning analysis of OCT angiography," *Trans. Vis. Sci. Technol.* **11**(7), 10–13 (2022).

204. P. Zang, T. T. Hormel, T. S. Hwang, S. T. Bailey, D. Huang, and Y. Jia, "Deep-learning–aided diagnosis of diabetic retinopathy, age-related macular degeneration, and glaucoma based on structural and angiographic OCT," *Ophthalmol. Sci.* **3**(1), 100245 (2023).
205. P. Zang, T. T. Hormel, J. Wang, Y. Guo, S. T. Bailey, C. J. Flaxel, D. Huang, T. S. Hwang, and Y. Jia, "Interpretable diabetic retinopathy diagnosis based on biomarker activation map," [arXiv](#), arXiv:2212.06299 (2022).